

# COMBINATORIAL COBORDISM MAPS IN HAT HEEGAARD FLOER THEORY

ROBERT LIPSHITZ, CIPRIAN MANOLESCU, AND JIAJUN WANG

ABSTRACT. In a previous paper, Sarkar and the third author gave a combinatorial description of the hat version of Heegaard Floer homology for three-manifolds. Given a cobordism between two three-manifolds, there is an induced map between their Heegaard Floer homologies. Here we present a procedure for finding the ranks of these maps combinatorially, in the hat version.

## 1. INTRODUCTION

In their papers [5], [6], [7], Ozsváth and Szabó constructed a decorated topological quantum field theory (TQFT) in  $3 + 1$  dimensions, called Heegaard Floer theory. (Strictly speaking, the axioms of a TQFT need to be altered slightly.) In its simplest version (called hat), to a closed, connected, oriented three-manifold  $Y$  and a  $\text{Spin}^c$  structure  $\mathfrak{s}$  on  $Y$  one associates a vector space  $\widehat{HF}(Y, \mathfrak{s})$  over the field  $\mathbb{F} = \mathbb{Z}/2\mathbb{Z}$ . Also, to a connected, oriented four-dimensional cobordism from  $Y_1$  to  $Y_2$  decorated with a  $\text{Spin}^c$  structure  $\mathfrak{t}$ , one associates a map

$$\widehat{F}_{W, \mathfrak{t}} : \widehat{HF}(Y_1, \mathfrak{t}|_{Y_1}) \rightarrow \widehat{HF}(Y_2, \mathfrak{t}|_{Y_2}).$$

The original definitions of the vector spaces  $\widehat{HF}$  and the maps  $\widehat{F}$  involved counting pseudo-holomorphic disks and triangles in symmetric products of a Riemann surface, which are related to the three-manifolds and cobordisms involved via Heegaard diagrams. In [9], Sarkar and the third author showed that every three-manifold admits a Heegaard diagram that is nice in the following sense: the curves split the diagram into elementary domains, all but one of which are bigons or rectangles. Using such a diagram, holomorphic disks in the symmetric product can be counted combinatorially, and the result is a combinatorial description of  $\widehat{HF}(Y)$  for any  $Y$ , as well as of the hat version of Heegaard Floer homology of null homologous knots and links in any three-manifold  $Y$ . A similar result was obtained in [2] for all versions of the Heegaard Floer homology of knots and links in the three-sphere.

The goal of this paper is to give a combinatorial procedure for calculating the ranks of the maps  $\widehat{F}_{W, \mathfrak{s}}$ . Roughly, the construction is as follows. The cobordism  $W$  is decomposed into a sequence of one-handle additions, two-handle additions, and three-handle additions. The maps induced by the one-handle additions are rather simple, being determined by the action of the first homology group on the Heegaard Floer homology of the final manifold; a corresponding statement holds for the three-handle additions. The only nontrivial part, then, is the two-handle additions. For these, we show that they can be represented by a multi-pointed triple Heegaard diagrams of a special form, in which all elementary domains that do not contain basepoints are bigons, triangles, or rectangles. In such diagrams all holomorphic triangles of Maslov index zero can be counted algorithmically, thus giving a combinatorial description of the map on  $\widehat{HF}$ .

We remark that in order to turn  $\widehat{HF}$  into a fully combinatorial TQFT, one ingredient is missing: naturality. Given two different nice diagrams for a three-manifold, the results of [5] show that the

---

RL was supported by an NSF Mathematical Sciences Postdoctoral Research Fellowship.

CM was supported by a Clay Research Fellowship.

JW was partially supported by the NSF Holomorphic Curves FRG grant 0244663.

resulting groups  $\widehat{HF}$  are isomorphic. However, there is not yet a combinatorial description of this isomorphism. Thus, while the results of this paper give an algorithmic procedure for computing the rank of a map  $\widehat{F}_{W,s}$ , the map itself is determined combinatorially only up to automorphisms of the image and the target.

The paper is organized as follows. In Section 2, we define a multi-pointed triple Heegaard diagram to be nice if all non-punctured elementary domains are bigons, triangles, or rectangles, and show that in a nice diagram holomorphic triangles can be counted combinatorially.<sup>1</sup> We then turn to the description of the map induced by two-handle additions. For the sake of clarity, in Section 3 we explain in detail the case of adding a single two-handle: we show that its addition can be represented by a nice triple Heegaard diagram with a single basepoint and, therefore, the induced map on  $\widehat{HF}$  admits a combinatorial description. We then explain how to modify the arguments to work in the case of several two-handle additions. This modification uses triple Heegaard diagrams with several basepoints. Finally, in Section 4, we discuss the additions of one- and three-handles, and put the various steps together.

**Acknowledgments.** We would like to thank Peter Ozsváth and Zoltán Szabó for helpful conversations and encouragement. In particular, several key ideas in the proof were suggested to us by Peter Ozsváth.

This work was done while the third author was an exchange graduate student at Columbia University. He is grateful to the Columbia math department for its hospitality. He would also like to thank his advisors, Robion Kirby and Peter Ozsváth, for their continuous guidance and support.

---

<sup>1</sup>Sucharit Sarkar has independently obtained this result (Proposition 2.3 below) in [8], using slightly different methods.

## 2. HOLOMORPHIC TRIANGLES IN NICE TRIPLE HEEGAARD DIAGRAMS

The goal of this section is to show that under an appropriate condition (niceness) on triple Heegaard diagrams, the counts of holomorphic triangles in the symmetric product are combinatorial.

**2.1. Preliminaries.** We start by reviewing some facts from Heegaard Floer theory. A triple Heegaard diagram  $\mathcal{H} = (\Sigma, \alpha, \beta, \gamma)$  consists of a surface  $\Sigma$  of genus  $g$  together with three  $(g+k)$ -tuples of pairwise disjoint embedded curves  $\alpha = \{\alpha_1, \dots, \alpha_{g+k}\}$ ,  $\beta = \{\beta_1, \dots, \beta_{g+k}\}$ ,  $\gamma = \{\gamma_1, \dots, \gamma_{g+k}\}$  in  $\Sigma$  such that the span of each  $(g+k)$ -tuple of curves in  $H_1(\Sigma)$  is  $g$ -dimensional. If we forget one set of curves (for example  $\gamma$ ), the result is an (ordinary) Heegaard diagram  $(\Sigma, \alpha, \beta)$ .

By the condition on the spans,  $\Sigma \setminus \alpha$ ,  $\Sigma \setminus \beta$  and  $\Sigma \setminus \gamma$  each has  $k+1$  connected components. By a multi-pointed triple Heegaard diagram  $(\mathcal{H}, \mathbf{z})$ , then, we mean a triple Heegaard diagram  $\mathcal{H}$  as above together with a set  $\mathbf{z} = \{z_1, \dots, z_{k+1}\} \subset \Sigma$  of  $k+1$  points in  $\Sigma$  which do not lie on any of the  $\alpha, \beta$ , or  $\gamma$  curves, and so that exactly one  $z_i$  lies in each connected component of  $\Sigma \setminus \alpha$ ,  $\Sigma \setminus \beta$  and  $\Sigma \setminus \gamma$ .

To a triple Heegaard diagram  $(\Sigma, \alpha, \beta, \gamma, \mathbf{z})$  one can associate three three-manifolds  $Y_{\alpha, \beta}$ ,  $Y_{\beta, \gamma}$  and  $Y_{\alpha, \gamma}$  and a four-manifold  $W_{\alpha, \beta, \gamma}$  such that  $\partial W_{\alpha, \beta, \gamma} = -Y_{\alpha, \beta} \cup -Y_{\beta, \gamma} \cup Y_{\alpha, \gamma}$ ; see [5].

Associated to a three-manifold  $Y_{\alpha, \beta}$  is the Heegaard-Floer homology group  $\widehat{HF}(Y_{\alpha, \beta})$ . This was defined using a Heegaard diagram with a single basepoint in [5]. In [3], Ozsváth and Szabó associated to the data  $(\Sigma, \alpha, \beta, \mathbf{z})$ , called a multi-pointed Heegaard diagram, a Floer homology group  $\widehat{HF}(\Sigma, \alpha, \beta, \mathbf{z})$  by counting holomorphic disks in  $\text{Sym}^{g+k}(\Sigma \setminus \mathbf{z})$  with boundary on the tori  $\mathbb{T}_\alpha = \alpha_1 \times \dots \times \alpha_{g+k}$  and  $\mathbb{T}_\beta = \beta_1 \times \dots \times \beta_{g+k}$ . It is not hard to show that

$$(1) \quad \widehat{HF}(\Sigma, \alpha, \beta, \mathbf{z}) \cong \widehat{HF}(Y_{\alpha, \beta}) \otimes H_*(T^k).$$

(Here,  $T^k$  is the  $k$ -torus, and  $H_*(T^k)$  means ordinary (singular) homology.) These homology groups decompose as a direct sum over  $\text{Spin}^c$ -structures on  $Y_{\alpha, \beta}$ ,

$$\widehat{HF}(Y_{\alpha, \beta}) \cong \bigoplus_{\mathfrak{s} \in \text{Spin}^c(Y_{\alpha, \beta})} \widehat{HF}(Y_{\alpha, \beta}, \mathfrak{s}).$$

More generally, there is a decomposition

$$\widehat{HF}(\Sigma, \alpha, \beta, \mathbf{z}) \cong \bigoplus_{\mathfrak{s} \in \text{Spin}^c(Y_{\alpha, \beta})} \widehat{HF}(\Sigma, \alpha, \beta, \mathbf{z}, \mathfrak{s}) \cong \bigoplus_{\mathfrak{s} \in \text{Spin}^c(Y_{\alpha, \beta})} \left( \widehat{HF}(Y_{\alpha, \beta}, \mathfrak{s}) \otimes H_*(T^k) \right).$$

Associated to the four-manifold  $W_{\alpha, \beta, \gamma}$ , together with a  $\text{Spin}^c$ -structure  $\mathfrak{t}$  on  $W_{\alpha, \beta, \gamma}$ , is a map  $\hat{F}_{W, \mathfrak{t}} : \widehat{HF}(Y_{\alpha, \beta}, \mathfrak{t}|_{Y_{\alpha, \beta}}) \otimes \widehat{HF}(Y_{\beta, \gamma}, \mathfrak{t}|_{Y_{\beta, \gamma}}) \rightarrow \widehat{HF}(Y_{\alpha, \gamma}, \mathfrak{t}|_{Y_{\alpha, \gamma}})$ . This was defined using a triple Heegaard diagram with a single basepoint in [5] and [7]. The definition, which involves counting holomorphic triangles in  $\text{Sym}^g(\Sigma \setminus \mathbf{z})$  with boundary on  $\mathbb{T}_\alpha$ ,  $\mathbb{T}_\beta$  and  $\mathbb{T}_\gamma$ , extends to the case of more basepoints, by replacing  $\text{Sym}^g$  by  $\text{Sym}^{g+k}$ . It is easy to see that these maps are compatible with the isomorphism (1), in the sense that the following diagram commutes:

$$\begin{array}{ccc} \left( \widehat{HF}(Y_{\alpha, \beta}, \mathfrak{t}|_{Y_{\alpha, \beta}}) \otimes H_*(T^k) \right) \otimes \left( \widehat{HF}(Y_{\beta, \gamma}, \mathfrak{t}|_{Y_{\beta, \gamma}}) \otimes H_*(T^k) \right) & \longrightarrow & \widehat{HF}(Y_{\alpha, \gamma}, \mathfrak{t}|_{Y_{\alpha, \gamma}}) \otimes H_*(T^k) \\ \downarrow \cong & & \downarrow \cong \\ \widehat{HF}(\Sigma, \alpha, \beta, \mathbf{z}, \mathfrak{t}|_{Y_{\alpha, \beta}}) \otimes \widehat{HF}(\Sigma, \beta, \gamma, \mathbf{z}, \mathfrak{t}|_{Y_{\beta, \gamma}}) & \xrightarrow{\hat{F}_{\Sigma, \alpha, \beta, \gamma, \mathbf{z}, \mathfrak{t}}} & \widehat{HF}(\Sigma, \alpha, \gamma, \mathbf{z}, \mathfrak{t}|_{Y_{\alpha, \gamma}}). \end{array}$$

Here, the map in the first row is  $\hat{F}_{W, \mathfrak{t}}$  on the  $\widehat{HF}$ -factors and the intersection product  $H_*(T^k) \otimes H_*(T^k) \rightarrow H_*(T^k)$  on the  $H_*(T^k)$ -factors. The proof that the diagram commutes follows from the same ideas as in [3]: after some isotopies, handleslides, and stabilizations, we can assume that the multi-pointed triple Heegaard diagram decomposes as a connected sum of  $k+1$  pieces, where  $k$  of the pieces are spheres with one basepoint and three isotopic curves (one  $\alpha$ , one  $\beta$  and one  $\gamma$ ). Each

of these  $k$  pieces contributes a  $H_*(S^1)$  to the  $H_*(T^k) = (H_*(S^1))^{\otimes k}$  factors above; moreover, a local computation shows that the triangles induce intersection product maps  $H_*(S^1) \otimes H_*(S^1) \rightarrow H_*(S^1)$ , which tensored together give the intersection product on  $H_*(T^k)$ .

**2.2. Index formulas.** Fix a triple Heegaard diagram  $\mathcal{H} = (\Sigma, \alpha, \beta, \gamma)$  as above. The complement of the  $3(g+k)$  curves in  $\Sigma$  has several connected components, which we denote by  $D_1, \dots, D_N$  and call *elementary domains*.

The *Euler measure* of an elementary domain  $D \subset \Sigma$  is

$$e(D) = \chi(D) - \frac{\# \text{ vertices of } D}{4}.$$

A *domain* in  $\Sigma$  is a two-chain  $D = \sum a_i D_i$  with  $a_i \in \mathbb{Z}$ . Its Euler measure is simply

$$e(D) = \sum_{i=0}^N a_i e(D_i).$$

As mentioned above, the maps  $\hat{F}_{\Sigma, \alpha, \beta, \gamma, \mathbf{z}, \mathbf{t}}$  induced by the triple Heegaard diagram  $\mathcal{H}$  are defined by counting holomorphic triangles in  $\text{Sym}^{g+k}(\Sigma)$  with respect to a suitable almost complex structure. According to the cylindrical formulation from [1], this is equivalent to counting certain holomorphic embeddings  $u : S \rightarrow \Delta \times \Sigma$ , where  $S$  is a Riemann surface (henceforth called the source) with some marked points on the boundary (which we call corners), and  $\Delta$  is a fixed disk with three marked points on the boundary. The maps  $u$  are required to satisfy certain boundary conditions, and to be generically  $(g+k)$ -to-1 when post-composed with the projection  $\pi_\Delta : \Delta \times \Sigma \rightarrow \Delta$ . More generally, we will consider such holomorphic maps  $u : S \rightarrow \Delta \times \Sigma$  which are generically  $m$ -to-1 when post-composed with  $\pi_\Delta$ ; these correspond to holomorphic triangles in  $\text{Sym}^m(\Sigma)$ , where  $m$  can be any non-negative integer. We will be interested in the discussion of the index from [1]. Although this discussion was carried-out in the case  $k=0$ ,  $m=g$ , it applies equally well in the case of arbitrary  $k$  and  $m$  with only notational changes.

In the cylindrical formulation, one works with an almost complex structure on  $\Delta \times \Sigma$  so that the projection  $\pi_\Delta$  is holomorphic, and the fibers of  $\pi_\Sigma$  are holomorphic. It follows that for  $u : S \rightarrow \Delta \times \Sigma$  holomorphic,  $\pi_\Delta \circ u$  is a holomorphic branched cover. The map  $\pi_\Sigma \circ u$  need not be holomorphic, but since the fibers are holomorphic,  $\pi_\Sigma \circ u$  is a branched map. Fix a model for  $\Delta$  in which the three marked points are  $90^\circ$  corners, and a conformal structure on  $\Sigma$  with respect to which the intersections between  $\alpha$ -,  $\beta$ - and  $\gamma$ -curves are all right angles. Since  $u$  is holomorphic, the conformal structure on  $S$  is induced via  $\pi_\Delta \circ u$  from the conformal structure on  $\Delta$ . It makes sense, therefore, to talk about branch points of  $\pi_\Sigma \circ u$  on the boundary and at the corners, as well as in the interior. Generically, while there may be branch points of  $\pi_\Sigma \circ u$  on the boundary of  $S$ , there will not be branch points at the corners.

Suppose  $u : S \rightarrow \Delta \times \Sigma$  is as above. Denote by  $\pi_\Sigma : \Delta \times \Sigma \rightarrow \Sigma$  the projection to  $\Sigma$ . There is an associated domain  $D(u)$  in  $\Sigma$ , where the coefficient of  $D_i$  in  $D(u)$  is the local multiplicity of  $\pi_\Sigma \circ u$  at any point in  $D_i$ . By [1, p. 1018], the *index* of the linearized  $\bar{\partial}$  operator at the holomorphic map  $u$  is given by

$$(2) \quad \mu(u) = 2e(D(u)) - \chi(S) + \frac{m}{2}.$$

For simplicity, we call this the index of  $u$ .

Note that, by the Riemann-Hurwitz formula:

$$(3) \quad \chi(S) = e(D(u)) + \frac{3m}{4} - \text{br}(u),$$

where  $\text{br}(u)$  is the ramification index (number of branch points counted with multiplicity) of  $\pi_\Sigma \circ u$ . (Here, branch points along the boundary count as half an interior branch point.) From (2) and (3)

we get an alternate formula for the index:

$$(4) \quad \mu(u) = e(D(u)) + \text{br}(u) - \frac{m}{4}.$$

A combinatorial formula for the index, purely in terms of  $D(u)$ , was found by Sarkar in [8]. However, we will not use it here.

**2.3. Nice triple diagrams.** Fix a multi-pointed triple Heegaard diagram  $(\mathcal{H}, \mathbf{z}) = (\Sigma, \boldsymbol{\alpha}, \boldsymbol{\beta}, \boldsymbol{\gamma}, \mathbf{z})$ . Recall that a domain is a linear combination of connected components of  $\Sigma \setminus (\boldsymbol{\alpha} \cup \boldsymbol{\beta} \cup \boldsymbol{\gamma})$ . The *support* of a domain is the union of those components with nonzero coefficients. If the support of a domain  $D$  contains at least one  $z_i$  then  $D$  is called *punctured*; otherwise it is called *unpunctured*.

**Definition 2.1.** *An elementary domain is called **good** if it is a bigon, a triangle, or a rectangle, and **bad** otherwise. The multi-pointed triple Heegaard diagram  $(\mathcal{H}, \mathbf{z})$  is called **nice** if every unpunctured elementary domain is good.*

This is parallel to the definition of nice Heegaard diagrams (with just two sets of curves) from [9]. A multi-pointed Heegaard diagram  $(\Sigma, \boldsymbol{\alpha}, \boldsymbol{\beta}, \mathbf{z})$  is called *nice* if, among the connected components of  $\Sigma \setminus (\boldsymbol{\alpha} \cup \boldsymbol{\beta})$ , all unpunctured ones are either bigons or squares.

Note that a bigon, a triangle, and a rectangle have Euler measure  $\frac{1}{2}$ ,  $\frac{1}{4}$ , and 0, respectively. Since  $e$  is additive, every unpunctured domain (not necessarily elementary) in a nice diagram must have nonnegative Euler measure. A quick consequence of this is the following:

**Lemma 2.2.** *If  $(\Sigma, \boldsymbol{\alpha}, \boldsymbol{\beta}, \boldsymbol{\gamma}, \mathbf{z})$  is a nice triple Heegaard diagram, then if we forget one set of curves (for example,  $\boldsymbol{\gamma}$ ), the resulting Heegaard diagram  $(\Sigma, \boldsymbol{\alpha}, \boldsymbol{\beta}, \mathbf{z})$  is also nice.*

In order to define the triangle maps it is necessary to assume the triple Heegaard diagram is weakly admissible in the sense of [5, Definition 8.8]. In fact, nice diagrams are automatically weakly admissible, cf. Corollary 3.2 below.

Our goal is to give a combinatorial description of the holomorphic triangle counts for nice triple diagrams.

**Proposition 2.3.** *Let  $(\mathcal{H}, \mathbf{z})$  be a nice multi-pointed triple Heegaard diagram. Let  $u : S \rightarrow \Delta \times \Sigma$  be a holomorphic map of the kind occurring in the definition of  $\hat{F}_{\boldsymbol{\alpha}, \boldsymbol{\beta}, \boldsymbol{\gamma}, \mathbf{z}, \mathbf{t}}$ . In particular, assume  $u$  is an embedding, of index zero, and such that the image of  $\pi_\Sigma \circ u$  is an unpunctured domain. Then  $S$  is a disjoint union of  $m$  triangles, and the restriction of  $\pi_\Sigma \circ u$  to each component of  $S$  is an embedding.*

*Proof.* Since the image of  $\pi_\Sigma \circ u$  is unpunctured, we have  $e(D(u)) \geq 0$ . By (2), we get

$$\chi(S) \geq \frac{m}{2} > 0.$$

This means that at least one component of  $S$  is topologically a disk. Let  $S_0$  be such a component. It is a polygon with  $3l$  vertices. We will show that  $l = 1$ , and that  $\pi_\Sigma \circ u|_{S_0}$  is an embedding.

Let us first show that  $S_0$  is a triangle. The index of the  $\bar{\partial}$  operator at a disconnected curve is the sum of the indices of its restrictions to each connected component. Therefore, in order for an index zero holomorphic curve to exist generically, the indices at every connected component, and in particular at  $S_0$ , must be zero. Applying (2) to  $u|_{S_0}$  we get

$$l = 2 - 4e(u|_{S_0}) \leq 2.$$

If  $l = 2$ , then by (4) we have  $\text{br}(u) \leq \frac{1}{2}$ . Hence, the map  $\pi_\Sigma \circ u$  has no interior branch points. If  $\text{br}(u) = 0$  then  $S_0$  is mapped diffeomorphically by  $\pi_\Sigma \circ u$  to  $\Sigma$ . The image must have negative Euler measure, which is a contradiction. So, suppose  $\text{br}(u) = 1/2$ . The preimages of the alpha, beta, and gamma curves cut  $S_0$  into several connected components. Without loss of generality, assume that the boundary branch point is mapped to an  $\alpha$ -circle. Then, along the corresponding

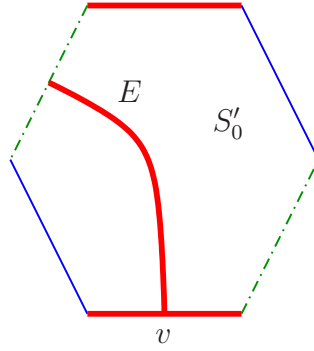


FIGURE 1. **A hexagon component of the source.** The preimages of the alpha, beta and gamma curves (here shown as thick, thin, and interrupted lines) give an embedded graph in the source  $S_0$ . A boundary branch point in the image corresponds to a valence three vertex  $v$  in the source.

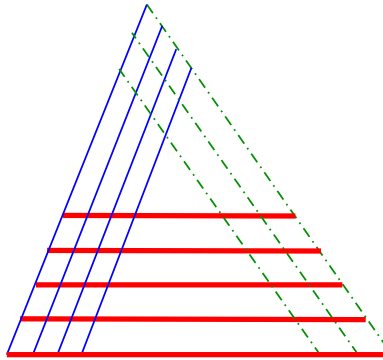


FIGURE 2. **An embedded triangle.** The thick (red) lines are  $\alpha$ 's, the thin (blue) ones  $\beta$ 's, and the interrupted (green) ones  $\gamma$ 's. We first show that this is the picture in the source  $S_0$ , and then that the same is true for the image of  $S_0$  in  $\Sigma$ , i.e. the images of all the pieces in the tiling are disjoint.

edge of  $S_0$  there is a valence three vertex  $v$ , as shown in Figure 1. Let  $E$  denote the edge in the interior of  $S_0$  meeting  $v$ . Since there is only one boundary branch point, the other intersection point of the edge  $E$  with  $\partial S_0$  is along the preimage of a  $\beta$ - or  $\gamma$ -circle. It follows that one of the connected components  $S'_0$  of  $S_0 \setminus E$  is a hexagon or heptagon. Smoothing the vertex  $v$  of  $S'_0$  we obtain a pentagon or hexagon which is mapped diffeomorphically by  $\pi_\Sigma \circ u$  to  $\Sigma$ . The image, then, has negative Euler measure, again a contradiction.

Therefore,  $l = 1$ , so  $S_0$  is a triangle. Furthermore, by (4),  $\text{br}(u) \leq 1/4$ , which means that there are no (interior or boundary) branch points at all. Thus, just as in the hypothetical hexagon case above, the preimages of the alpha, beta, and gamma curves must cut  $S_0$  into 2-gons, 3-gons, and 4-gons, all of whom have nonnegative Euler measure. Since the Euler measure of  $S_0$  is  $1/4$ , there can be no bigons; in fact,  $S_0$  must be cut into several rectangles and exactly one triangle. It is easy to see that the only possible tiling of  $S_0$  of this type is as in Figure 2, with several parallel preimages of segments on the alpha curves, several parallel beta segments, and several parallel gamma segments. We call the type of a segment ( $\alpha$ ,  $\beta$  or  $\gamma$ ) its color.

The tiling consists of one triangle and six different types of rectangles, according to the coloring of their edges in clockwise order (namely,  $\alpha\beta\alpha\gamma$ ,  $\gamma\alpha\gamma\beta$ ,  $\beta\alpha\beta\gamma$ ,  $\alpha\beta\alpha\beta$ ,  $\beta\gamma\beta\gamma$ , and  $\gamma\alpha\gamma\alpha$ ). We claim that the images of the interiors of each of these rectangles by  $\pi_\Sigma \circ u$  are disjoint.

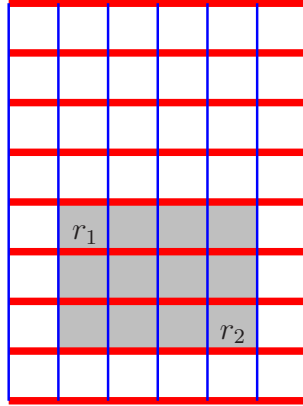


FIGURE 3. **Two  $\alpha\beta\alpha\beta$  rectangles in a grid.** If the rectangles  $r_1$  and  $r_2$  had the same image in  $\Sigma$  with a  $180^\circ$  turn, then the whole shaded rectangle would be mapped to  $\Sigma$  with a branch point.

Because of the coloring scheme, we can only conceivably have rectangles of the same type have the same image. Suppose that two different  $\alpha\beta\alpha\gamma$  rectangles from  $S_0$  have the same image in  $\Sigma$ . (The cases  $\gamma\alpha\gamma\beta$ ,  $\beta\alpha\beta\gamma$  are exactly analogous.) Let  $r_1$  and  $r_2$  be the two rectangles; suppose that  $r_1$  is closer to the central triangle than  $r_2$ , and  $r_2$  is closer to the  $\alpha$  boundary of  $S_0$ . Because of the way the rectangles are colored, the upper edge of  $r_1$  must have the same image as the upper edge of  $r_2$ . Hence the  $\alpha\beta\alpha\gamma$  rectangle right above  $r_1$  has the same image as the one right above  $r_2$ . Iterating this argument, at some point we get that the central triangle has the same image as some  $\alpha\beta\alpha\gamma$  rectangle, which is impossible.

Now suppose that two different  $\alpha\beta\alpha\beta$  rectangles,  $r_1$  and  $r_2$ , have the same image. (The cases  $\beta\gamma\beta\gamma$  and  $\gamma\alpha\gamma\alpha$  are exactly analogous.) There are two cases, according to whether the upper edge of  $r_1$  has the same image as the upper edge of  $r_2$ , or as the lower edge of  $r_2$ .

Suppose first that the upper edge of  $r_1$  has the same image as the upper edge of  $r_2$ . By the  $\beta$ -height of  $r_i$  we mean the minimal number of  $\beta$ -arcs that an arc in  $S \setminus \alpha$  starting in  $r_i$ , going up, and ending at a  $\gamma$ -arc must cross. (The diagram is positioned in the plane as in Figure 2.) Since  $\pi_\Sigma \circ u$  is a local homeomorphism, and  $r_1$  and  $r_2$  have the same image, it is clear that the  $\beta$ -height of  $r_1$  and the  $\beta$ -height of  $r_2$  are equal. By the  $\alpha$ -height of  $r_i$  we mean the minimal number of  $\alpha$ -arcs that an arc in  $S \setminus \beta$  starting in  $r_i$ , going right, and ending at a  $\gamma$ -arc must cross. Again, it is clear that the  $\alpha$ -heights of  $r_1$  and  $r_2$  must be equal. But this implies that  $r_1$  and  $r_2$  are equal.

Now, suppose that the upper edge of  $r_1$  has the same image as the lower edge of  $r_2$ . There is a unique rectangle  $R$  in  $S$  with boundary contained in  $\alpha \cup \beta$ , containing  $r_1$  and  $r_2$ , and with one corner the same as a corner of  $r_1$  and the opposite corner the same as a corner of  $r_2$ . It is easy to see that  $\pi_\Sigma \circ u$  maps antipodal points on the boundary of  $R$  to the same point in  $\Sigma$ . It follows that  $\pi_\Sigma \circ u|_{\partial R}$  is a two-fold covering map. But then  $\pi_\Sigma \circ u$  must have a branch point somewhere inside  $R$  – a contradiction. See Figure 3.

Finally, suppose some arc  $A$  on  $\partial S$  has the same image as some other arc  $A'$  in  $S$ . If  $A'$  is in the interior of  $S$  then any rectangle (or triangle) adjacent to  $A$  has the same image as some rectangle (or triangle) adjacent to  $A'$ . We have already ruled this out. If  $A'$  is on  $\partial S$ , then either any rectangle (or triangle) adjacent to  $A$  has the same image as some rectangle (or triangle) adjacent to  $A'$  or there is a branch point somewhere on  $\partial S$ . We have already ruled out both of these cases.

We have thus established that  $S_0$  is an embedded triangle. By forgetting  $S_0$ , we obtain a holomorphic map to  $\Delta \times \Sigma$ , still of index zero, but such that its post-composition with  $\pi_\Delta$  is generically  $(m-1)$ -to-1 rather than  $m$ -to-1. The result then follows by induction on  $m$ .  $\square$

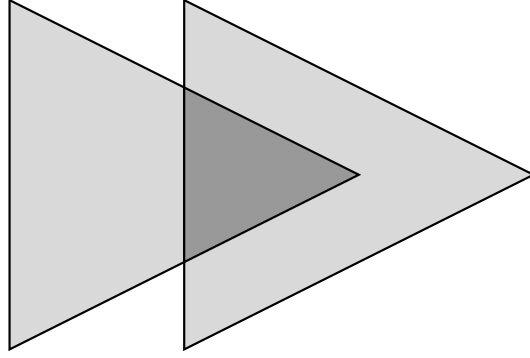


FIGURE 4. **Head to tail overlap.** A pair of embedded triangles  $T$  and  $T'$  overlap “head to tail” if their intersection  $T \cap T'$  consists of a single connected component, itself a triangle, which contains one vertex of one of the two triangles and no vertices of the other. In the picture, the two triangles are shaded; the intersection is darkly shaded. We have not colored the figure to indicate that any of the three possible coloring schemes is allowed; however, in all three cases, parallel segments in the figure are of the same type ( $\alpha$ ,  $\beta$  or  $\gamma$ ).

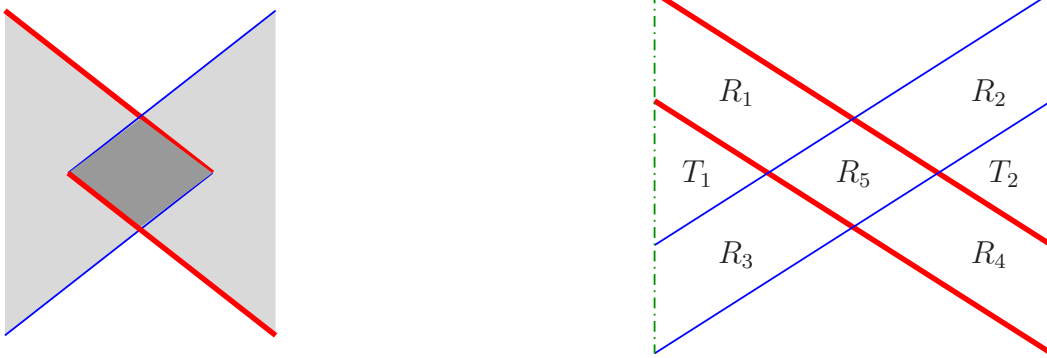


FIGURE 5. **Head to head overlap.** If  $T$  and  $T'$  intersect around their  $\alpha\beta$  vertices as on the left of the figure (where the intersection is shown by a darker shading), their union  $T \cup T'$  does not have index zero. This can be seen using an alternate decomposition of the domain  $T \cup T'$  as  $T_1 \cup T_2 \cup R \cup R'$ , where  $R = R_1 \cup R_4 \cup R_5$  and  $R' = R_2 \cup R_3 \cup R_5$ , where  $T_i (i = 1, 2)$  and  $R_j (j = 1, \dots, 5)$  are the domains shown on the right. (Note that on the right, there might be overlaps in other parts of the diagram; for example, we can have the situation in Figure 6.) The cases of  $\alpha\gamma$  or  $\beta\gamma$  head to head overlaps are similar.

Observe that, in Proposition 2.3 above, even though each of the  $m$  triangles is embedded, some of their domains may overlap. It turns out that they may do so only in a specific way, however:

**Lemma 2.4.** *Suppose  $A$  is an index zero homology class represented by a union of embedded holomorphic triangles, in a nice triple diagram. Suppose the union of triangles corresponds to an embedded holomorphic curve in  $\Delta \times \Sigma$ . Then any two triangles in  $A$  are either disjoint in  $\Sigma$  or overlap in  $\Sigma$  “head to tail” as shown in Figure 4.*

*Proof.* Let  $T$  and  $T'$  be two of the triangles in the domain  $A$ . For a generic representative of  $A$  to exist, the pair must also have index zero, and be embedded in  $\Delta \times \Sigma$ .

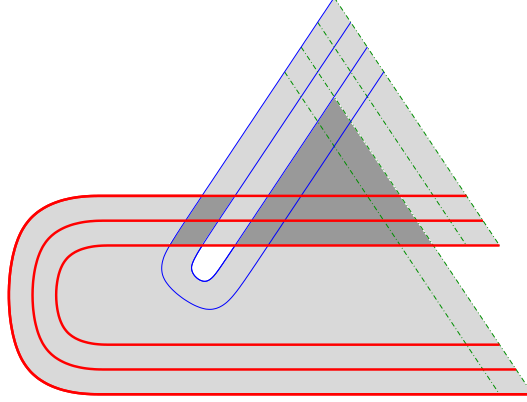


FIGURE 6. **A double overlap.** The two triangles (each shown lightly shaded) have a (darkly shaded) overlap with two connected components.

We already know that  $T$  and  $T'$  are tiled as in Figure 2. This strongly restricts how  $T$  and  $T'$  can overlap.

One way for  $T$  and  $T'$  to overlap is for  $T$  to be entirely contained inside  $T'$ . In this case, it is not hard to see that the two holomorphic triangles in  $\Delta \times \Sigma$  intersect in one interior point. Indeed, the intersection number of two holomorphic curves in a 4-manifold is invariant in families. If we deform the Heegaard diagram so that the boundary of  $T$  in  $\Sigma$  is a single point (i.e., the  $\alpha$ -,  $\beta$ - and  $\gamma$ -circles involved in  $\partial T$  intersect in an asterisk, with vertex the “triangle”  $T$ ) then obviously  $(T \cap T') \subset (\Delta \times \Sigma)$  is a single point. It follows that the same is true for the original triangles  $T$  and  $T'$ .

Another way that  $T$  and  $T'$  might overlap is “head to head” as shown on the left side of Figure 5. It is then possible to decompose  $T \cup T'$  into a pair of rectangles  $R$  and  $R'$ , and two new embedded triangles  $T$  and  $T'$ , as shown in Figure 5. An immersed rectangle in  $\Sigma$  has index at least 1, since it admits a generic holomorphic representative. So, each of  $R_1$  and  $R_2$  has index at least 1. Similarly, the pair of triangles  $T_1 \cup T_2$  has index at least 0. So, by additivity of the index, the whole domain has index at least 2 – a contradiction.

Using these two observations, and the rulings of  $T$  and  $T'$ , it is then elementary to check that the only possible overlap in index zero is “head to tail” as in Figure 4.  $\square$

It follows that, for a nice Heegaard diagram, we can combinatorially describe the generic holomorphic curves of index 0. If  $D$  is the domain of a generic holomorphic curve of index 0 then  $\partial D$  has  $m$  components, each of which bounds an embedded triangle in  $\Sigma$ . Each pair of triangles must either be disjoint or overlap as shown in Figure 4. Any such  $D$  clearly has a unique holomorphic representative with respect to a split complex structure  $j_\Delta \times j_\Sigma$  on  $\Delta \times \Sigma$ . Further, it is well known that these holomorphic curves are transversally cut out, and so persist if one takes a small perturbation of  $j_\Delta \times j_\Sigma$ . In summary, to count index zero holomorphic curves in  $\Delta \times \Sigma$  with respect to a generic perturbation of the split complex structure, it suffices to count domains  $D$  which are sums of  $m$  embedded triangles in  $\Sigma$ , overlapping as allowed in the statement of Lemma 2.4.

## 3. TWO-HANDLE ADDITIONS

In this section we describe an algorithm to get a nice triple Heegaard diagram for two-handle additions. For the most part we will focus on the case when we add a single two-handle. In the last subsection we will explain how the arguments generalize to several two-handles.

To keep language concise, in this section we will refer to elementary domains as *regions*.

**3.1. A property of nice Heegaard diagrams.** Let  $(\Sigma, \alpha, \beta, \mathbf{z})$  be a multi-pointed (ordinary) Heegaard diagram. Recall that the diagram is called nice if all unpunctured regions are either bigons or squares.

**Lemma 3.1.** *On a nice Heegaard diagram  $(\Sigma, \alpha, \beta, \mathbf{z})$ , for any alpha circle  $\alpha_i$  with an arbitrary orientation, there exists a punctured region  $D$  which contains an edge  $e$  belonging to  $\alpha_i$ , and such that  $D$  is on the left of  $\alpha_i$ . The same conclusion holds for each beta circle.*

*Proof.* Suppose a half-neighborhood on the left of the alpha circle  $\alpha_i$  is disjoint from all the punctured regions. Then immediately to the left of  $\alpha_i$  we only have good regions. There are two possibilities as indicated in Figure 7.

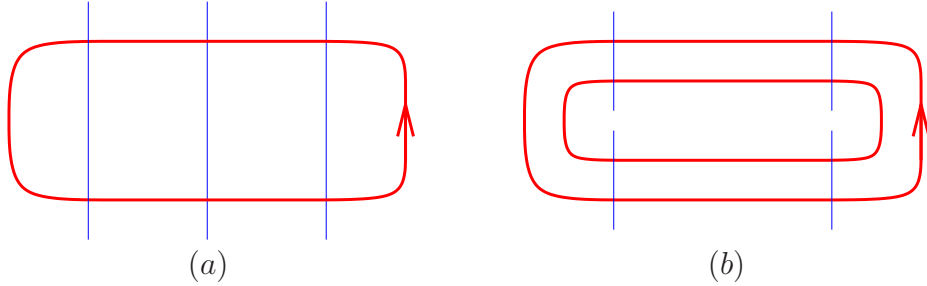


FIGURE 7. **Alpha curve not adjacent to the bad region.** The thick curves are alpha curves and the thin ones are beta curves.

If there is a bigon region on the left of  $\alpha_i$ , then the other edge is some beta edge  $\beta_j$ . The region on the other side of  $\beta_j$  must be a bigon region or a square since otherwise we would have a punctured region on the left of  $\alpha_i$ . If we reach a square, we continue to consider the next region. Eventually we will reach a bigon region since the number of regions are finite and we will not reach the same region twice. All regions involved form a disk bounded by  $\alpha_i$  (as in Figure 7 (a)). In particular, this means  $\alpha_i$  is null homologous. This contradicts the fact that the  $g$  alpha circles represent linearly independent classes in  $H_1(\Sigma \setminus \mathbf{z})$ .

In the second case, there are no bigon regions. Then on the left of  $\alpha_i$ , we see a chain of squares, as in Figure 7 (b). The opposite edges on these squares give another alpha circle, say  $\alpha_j$ . Then  $\alpha_i$  and  $\alpha_j$  are homologous to each other in  $H_1(\Sigma \setminus \mathbf{z})$ . This contradicts the same fact as in the previous case.  $\square$

Recall that in order to define the triangle maps it is necessary for the triple Heegaard diagram to be weakly admissible in the sense of [5, Definition 8.8].

**Corollary 3.2.** *If  $(\Sigma, \alpha, \beta, \gamma, \mathbf{z})$  is a nice multi-pointed triple Heegaard diagram then  $(\Sigma, \alpha, \beta, \gamma, \mathbf{z})$  is weakly admissible.*

*Proof.* By definition, the diagram is weakly admissible if there are no nontrivial domains  $D$  supported in  $\Sigma \setminus \mathbf{z}$  with nonnegative multiplicity in all regions, and whose boundary is a linear combination of alpha, beta, and gamma curves. Suppose such a domain  $D$  exists, and consider a curve appearing with a nonzero multiplicity in  $\partial D$ . Without loss of generality, we can assume this is an

alpha curve, and all regions immediately to its left have positive multiplicity in  $D$ . By Lemma 2.2, the diagram  $(\Sigma, \alpha, \beta, \mathbf{z})$  is nice. Lemma 3.1 now gives a contradiction.  $\square$

**3.2. A single two-handle addition.** Let  $(Y, K)$  be a three-manifold together with a knot  $K \subset Y$ . We choose a singly pointed Heegaard diagram  $(\Sigma, \alpha, \beta, z)$  for  $Y$  together with an additional basepoint  $w \neq z \in \Sigma \setminus (\alpha \cup \beta)$  such that the two basepoints determine the knot as in [4]. After applying the algorithm from [9] to the Heegaard diagram, we can assume that the Heegaard diagram is nice, with  $D_z$  the (usually bad) region containing the basepoint  $z$ . Furthermore, the algorithm in [9] also ensures that  $D_z$  is a polygon.

We denote by  $D_w$  the region containing  $w$ ; note that either  $D_w = D_z$  or  $D_w$  is good. Throughout this section, we will suppose that  $D_w$  and  $D_z$  are two different regions, and that  $D_w$  is a rectangle. The case when  $D_w = D_z$  corresponds to surgery on the unknot, which is already well understood. The case when  $D_w$  is a bigon is similar to the rectangle case, but easier.

Let  $W$  be the four manifold with boundary obtained from  $Y \times [0, 1]$  by adding a two handle along  $K$  in  $Y \times \{1\}$ , with some framing.  $W$  gives a cobordism between  $Y$  and  $Y'$ , where  $Y'$  is obtained from  $Y$  by doing the corresponding surgery along  $K$ .

Now we are ready to describe our algorithm to get a nice triple Heegaard diagram for the cobordism  $W$ .

### Step 1. Making the knot embedded in the Heegaard diagram.

Let  $c$  be an embedded arc in  $\Sigma$  connecting  $z$  and  $w$  in the complement of beta curves, and  $c'$  be an embedded arc connecting  $z$  and  $w$  in the complement of alpha curves. The union of  $c$  and  $c'$  is a projection of the knot  $K \subset Y$  to the surface  $\Sigma$ , where  $\Sigma$  is viewed as a Heegaard surface in  $Y$ . For convenience, we will always assume that  $c$  and  $c'$  do not pass through any bigon regions, and never leave a rectangle by the same edge through which they entered; this can easily be achieved.

In this step, we modify the doubly pointed Heegaard diagram  $(\Sigma, \alpha, \beta, z, w)$  to make  $c \cup c'$  embedded in  $\Sigma$ , while preserving the niceness of the Heegaard diagram.

Typically,  $c$  and  $c'$  have many intersections. We modify the diagram inductively by stabilization at the first intersection  $p \in D_p$  on  $c'$  (going from  $z$  to  $w$ ) to remove that intersection, while making sure that the new diagram is still nice.

A neighborhood of  $c$  and the part on  $c'$  from  $z$  to  $p$  are shown in Figure 8. In the same picture, if we continue the chain of rectangles containing  $c$ , we will end up with a region  $D'$  which is either a bigon or the punctured region  $D_z$ .

To get rid of the intersection point  $p$ , we stabilize the diagram as in Figure 9. More precisely, we do a stabilization followed by some handleslides of the beta curves and an isotopy of the new beta curve. After these moves, the number of intersection points decreases by one and the diagram is still nice.

If we iterate this process, in the end we get a nice Heegaard diagram in which  $c$  and  $c'$  only intersect at their endpoints. Furthermore, the bad region  $D_z$  is still a polygon.

### Step 2. Adding twin gamma curves.

Our goal in Steps 2 and 3 is to describe a particular triple Heegaard diagram for the cobordism  $W$ . Starting with the  $\alpha$  and the  $\beta$  curves we already have, for each beta curve  $\beta_i$  we will add a gamma curve  $\gamma_i$  (called its twin) which is isotopic to  $\beta_i$  and intersects it in exactly two points. (After this, we will add some more curves in the next step.)

For any beta curve  $\beta_i$ , by Lemma 3.1 we can choose a region  $D_i$  so that  $D_i$  is adjacent to the punctured region  $D_z$  with the common edge on  $\beta_i$ . If  $D_i = D_z$ , then we add  $\gamma_i$  close and parallel to  $\beta_i$  as in Figure 10 (a), and make a finger move as in Figure 10 (b).

Suppose now that  $D_i$  is different from  $D_z$ . Then  $D_i$  has to be a good region.

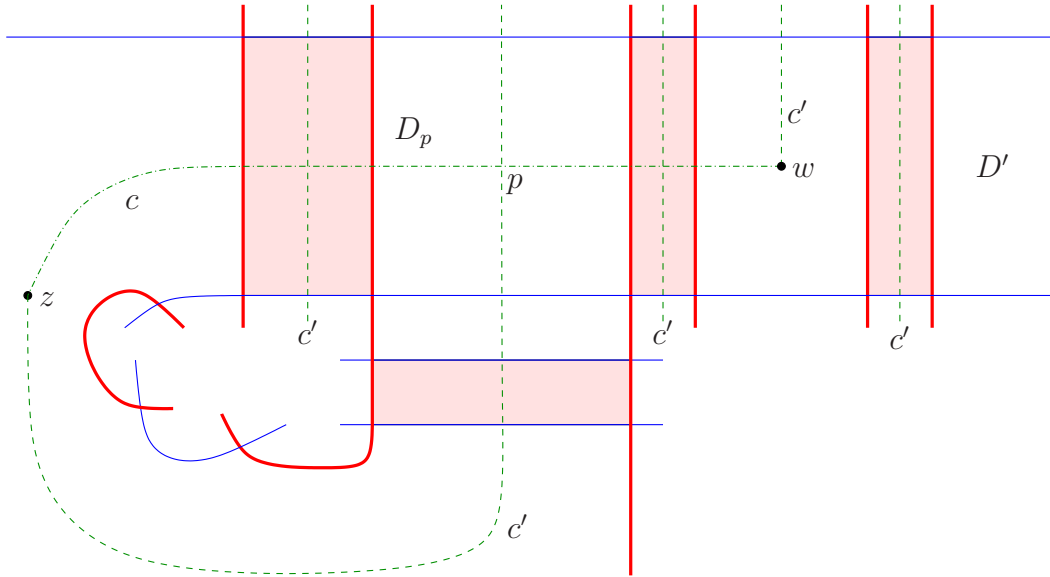


FIGURE 8. **Projection of the knot to the Heegaard surface.** As usual, the thick lines are alpha curves, and the thin lines are betas. The point  $p$  is the first on the dashed  $c'$  curve (starting from  $z$ ) where an intersection with  $c$  takes place. The light shading in the upper three domains indicates that there might be more parallel copies of alpha curves or parts of the  $c'$  curve. Similarly, the light shading in the lower domain indicates the presence of an arbitrary number of parallel beta segments there. Note that some of the regions in the rightmost shaded domain on the top can coincide with some of the regions in the bottom shaded domain; however, this fact will not create any difficulties.

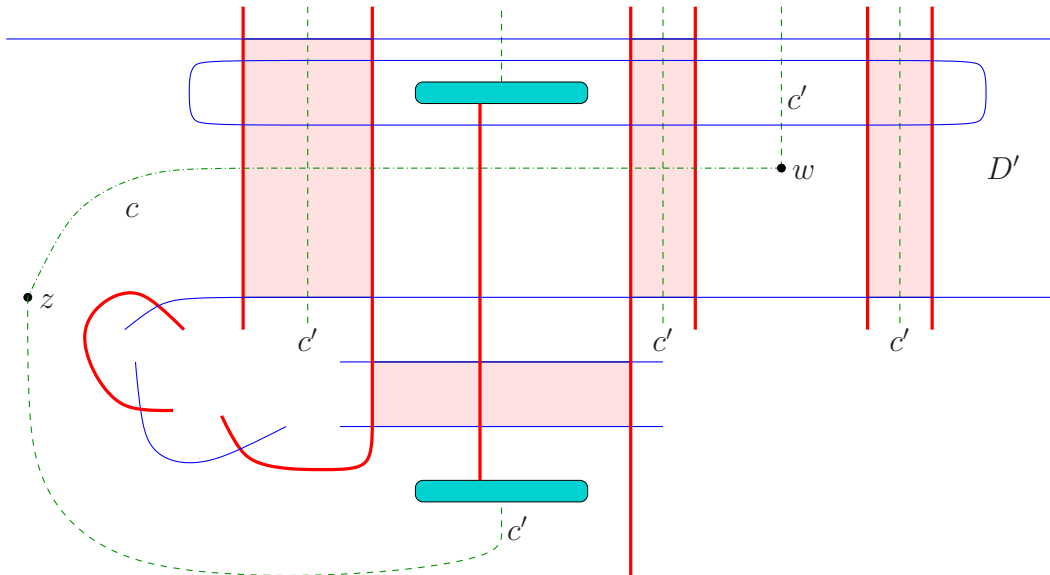
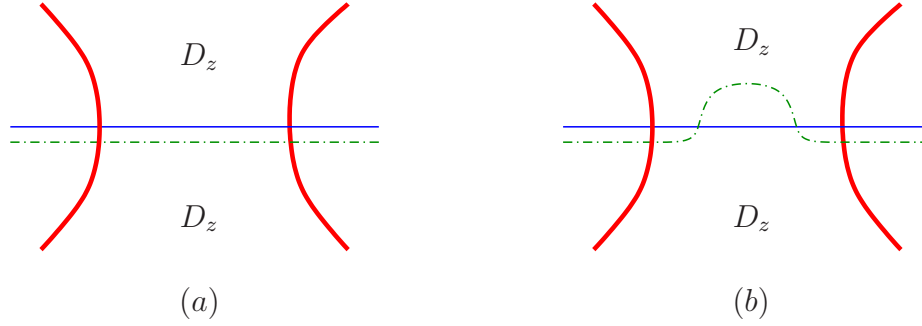


FIGURE 9. **Stabilizing at the intersection.** The two darkly shaded ovals are the two feet of the handled we added. In the stabilized picture, we stretch the new beta curve until it reaches the regions  $D_z$  and  $D'$ , so that the diagram is still nice.


 FIGURE 10. **Adding twin gamma curves - Case 1.**

Here and after, without further specification, we make the convention that the thick arcs are alpha arcs, the thin ones are beta arcs, and the interrupted ones are gamma arcs.

If  $D_i$  is not a bigon, since the complement of the beta curves in  $\Sigma$  is connected, we can connect  $D_i$  with  $D_z$  without intersecting beta curves, via an arc traversing a chain of rectangles, as indicated in the Figure 11. Then we do a finger move of the curve  $\beta_i$  as indicated in Figure 12.

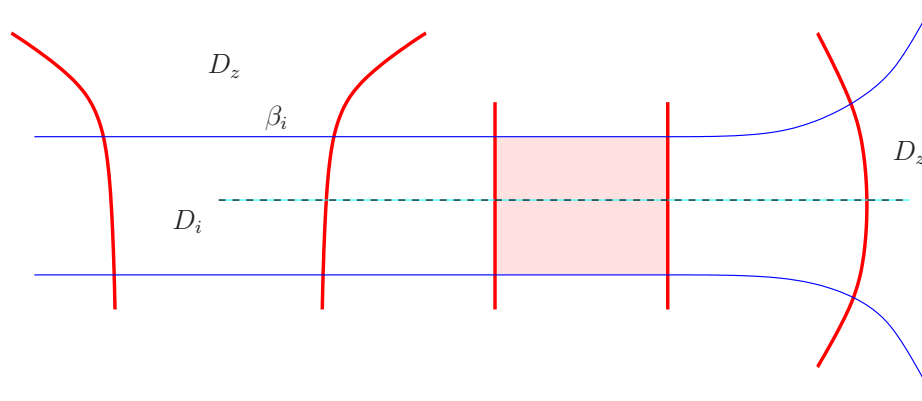


FIGURE 11. **An arc connecting  $D_i$  to  $D_z$ .** The shaded domain may contain several parallel alpha edges, and the dashed arc is the connecting arc.

Now we have a bigon region. We then add the gamma curve  $\gamma_i$  as shown in Figure 12.

Note that for each pair  $\beta_i$  and  $\gamma_i$ , we either have one sub-diagram of the form in Figure 10 (b), or one sub-diagram of the form in Figure 13. Observe also that during this process, no bad region other than  $D_z$  is created.

### Step 3. Stabilization and two-handle addition.

By Step 1, we can use arcs to connect  $z$  to  $w$  by paths in the complement of alpha curves, and in the complement of beta curves so that the two arcs do not intersection except for the end points  $w$  and  $z$ , and do not pass through any bigons. We will see two chains of squares, as indicated in Figure 14.

We do a stabilization of the Heegaard diagram by adding a handle with one foot in each of  $D_z$  and  $D_w$ . We add the additional beta circle  $\beta_{g+1}$  to be the meridian of the handle, which we push along  $c$  until it reaches  $D_z$ . We also push  $\beta_{g+1}$  through the opposite  $\alpha$ -edge of  $D_w$ , into the adjacent region. Then, we connect the two feet in the complement of alpha curves along  $c'$  and get a new alpha circle  $\alpha_{g+1}$ . Finally, we add the surgery gamma circle  $\gamma_{g+1}$  as in Figure 14. The result is a triple Heegaard diagram (with  $3(g + 1)$  curves) which represents surgery along the knot  $K \subset Y$ ,

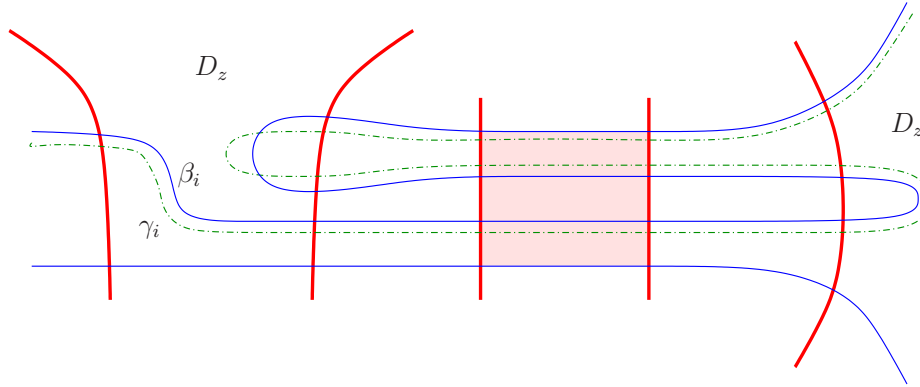


FIGURE 12. **Adding twin gamma curves - Case 2.** Before adding  $\gamma_i$ , we do the finger move shown here. Again, the shaded domain may contain several parallel alpha segments.

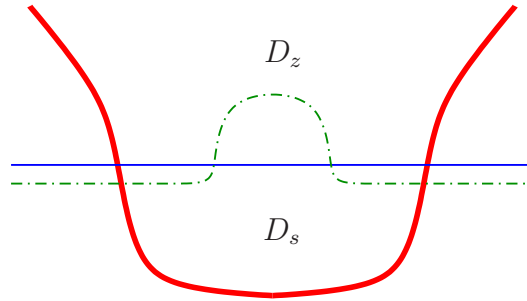


FIGURE 13. **Bigon between beta and gamma curves.** The region  $D_s$  will be dealt with in a special way in later steps.

with a particular framing; the framing is the sum of the number of twists of  $\gamma_{g+1}$  around the handle and a constant depending only on the original Heegaard diagram.

Note that, depending on the framing, the local picture around the two feet of the handle may also look like Figure 15, in which case instead of the octagon region  $D_*$  from Figure 14 we have two hexagon bad regions  $D_{*,1}$  and  $D_{*,2}$ .

After the stabilization,  $\alpha_{g+1}$  and  $\gamma_{g+1}$  separate  $D_z$  into several regions; among these,  $D_{z,1}$  and  $D_{z,2}$  are (possibly) bad but all other regions are good. We end up with a diagram with four (or five) bad regions:  $D_{z,1}$ ,  $D_{z,2}$ ,  $D_*$  (or  $D_{*,1}$  and  $D_{*,2}$ ), and  $D'$ . (In some cases,  $D_{z,1}$  or  $D_{z,2}$  might be good, or, if there is little winding of  $\gamma_{g+1}$ , some of  $D_*$ ,  $D_{z,1}$ , and  $D_{z,2}$  might coincide. The argument in these cases is a simple adaptation of the one we give below.) We will kill the badness of  $D'$ ,  $D_*$  (or  $D_{*,1}$  and  $D_{*,2}$ ), and one of  $D_{z,1}$  and  $D_{z,2}$ , while the remaining one ( $D_{z,2}$  or  $D_{z,1}$ ) will be the one containing the basepoint  $z$  for our final triple Heegaard diagram.

#### Step 4. Killing the bad region $D'$ .

We push the finger in  $D'$  across the opposite alpha edge until we reach a bigon,  $D_{z,1}$ ,  $D_{z,2}$ , or a region of type  $D_s$  as in Figure 13.

*Case 1. A bigon is reached.* In this case (Figure 16 (a)), our finger move will kill the badness of  $D'$ , as indicated in Figure 16 (b), and does not create any new bad regions.

*Case 2.  $D_{z,1}$  or  $D_{z,2}$  is reached.* Without loss of generality, we suppose that  $D_{z,1}$  is reached. In Step 5, we will kill the badness of  $D_{z,2}$ , and  $D_{z,1}$  will contain the basepoint  $z$  in the final triple

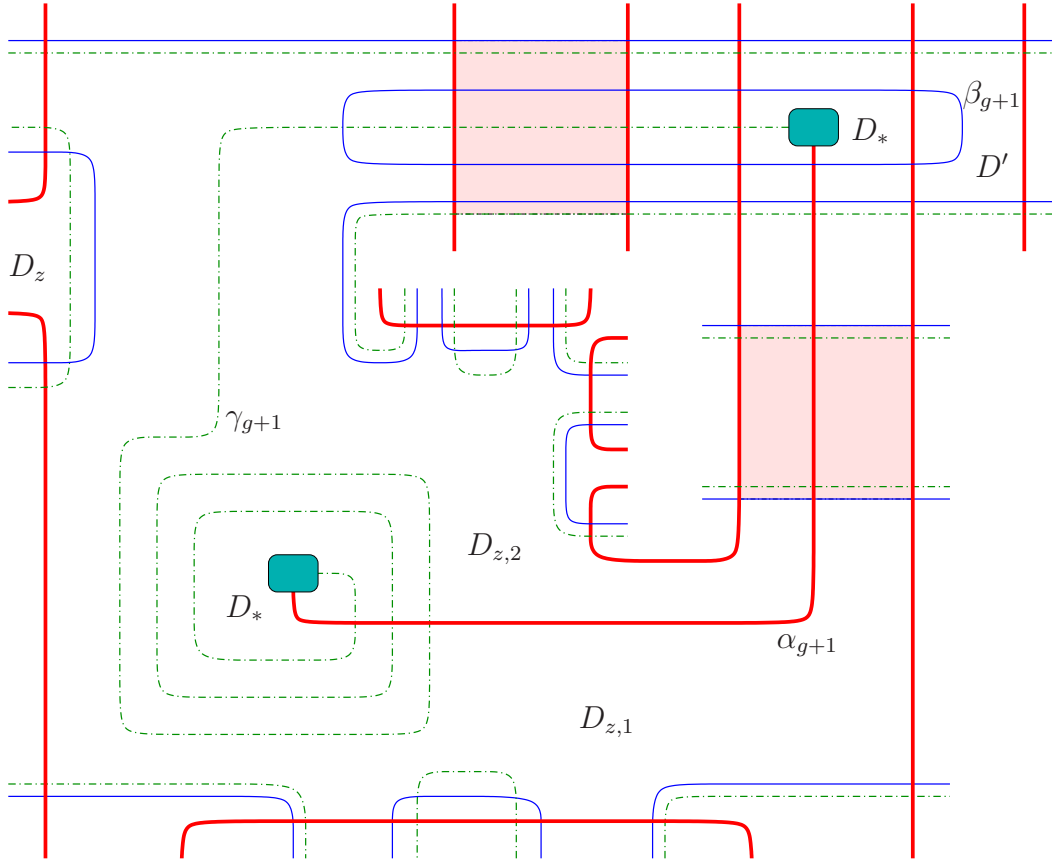


FIGURE 14. **Stabilization - Case 1.** The two small darkly shaded ovals are the two feet of the handle. The upper large lightly shaded area may have several parallel copies of alpha arcs, while the lower one may have several copies of beta and gamma arcs. The upper left  $D_z$  denotes either  $D_{z,1}$  or  $D_{z,2}$ ; such a domain can occur at various places on the boundaries of  $D_{z,1}$  or  $D_{z,2}$ , and it corresponds to Case 1 in Step 2.

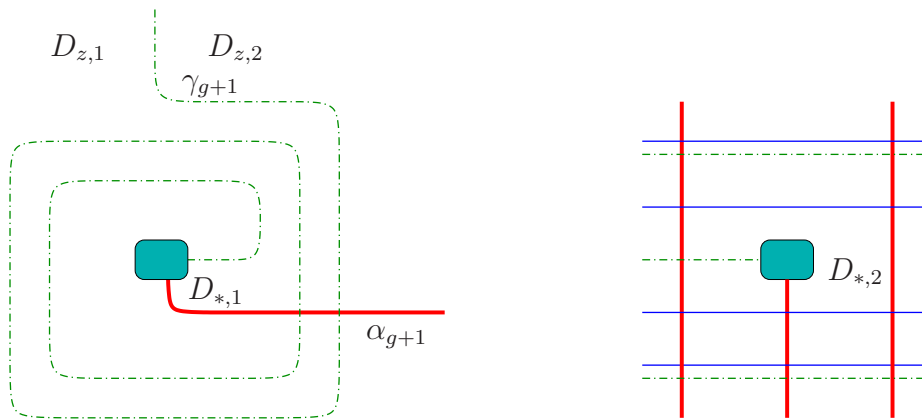


FIGURE 15. **Stabilization - Case 2.** If the  $\gamma_{g+1}$  twists around the handle in the opposite direction, we still have a picture similar to Figure 14. The only differences are in the neighborhoods of the two feet of the handle, which are shown here.

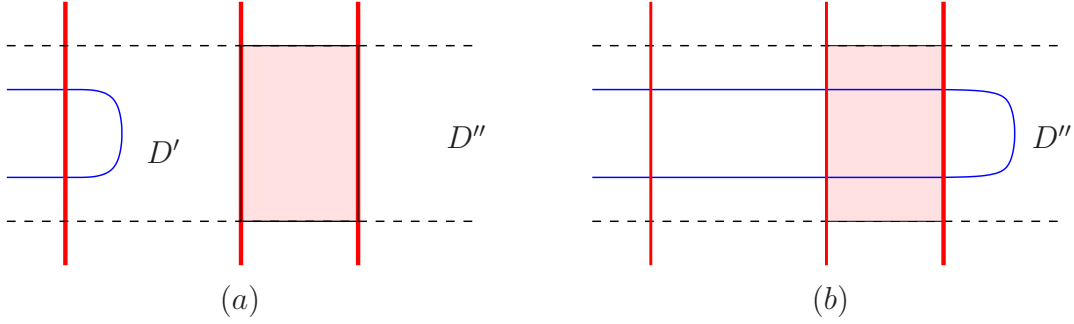


FIGURE 16. **Killing badness of  $D'$ : bigon,  $D_{z,1}$  or  $D_{z,2}$  case.** The thick arcs are alpha curves, the thin arcs represent  $\beta_{g+1}$ , and the dashed arcs can be either betas or gammas. The shaded part has several parallel alpha arcs. The rightmost region  $D''$  is a bigon,  $D_{z,1}$ , or  $D_{z,2}$ .

Heegaard diagram. The case in which we reach  $D_{z,2}$  is symmetric, with the winding in the opposite direction.

In either case, the finger move kills the badness of  $D'$ . As in Case 1, it does not create any new bad regions.

*Case 3. A region of type  $D_s$  is reached.* Let us suppose the rightmost region in Figure 13 is  $D_{z,1}$ . In Step 5, we will kill the badness of  $D_{z,2}$ , and  $D_{z,1}$  will contain the basepoint  $z$  in the final triple Heegaard diagram. The case when the rightmost region is  $D_{z,2}$  is symmetric.

The regions involved look like Figure 17. If on the left  $D_{z,1}$  is on top of  $D_{z,2}$ , we isotope the diagram to look as in Figure 18. The case when on the left of Figure 13  $D_{z,2}$  is on top of  $D_{z,1}$  is similar, except that we do the double finger move on the other side of  $\beta_{g+1}$ .

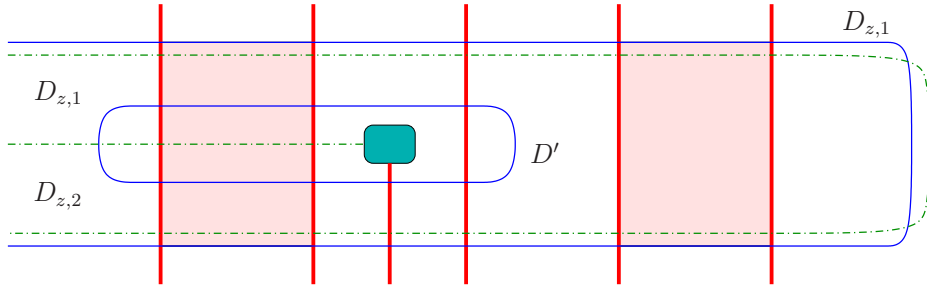


FIGURE 17. **Killing badness of  $D'$ :  $D_s$  type region - before.** The smaller shaded region is the foot of the handle inside  $D_w$ , while the larger two shaded regions may contain several parallel alpha arcs.

We have now killed the badness of  $D'$ . From now on we will assume that either we encountered Case 1 of this step, or we encountered Case 2 and we reached  $D_{z,1}$ , or we encountered Case 3 and the rightmost region was  $D_{z,1}$ . If we encountered Case 2 and we reached  $D_{z,2}$ , or we encountered Case 3 and the rightmost region was  $D_{z,2}$ , then in the next step we would kill  $D_{z,1}$  rather than  $D_{z,2}$ , but otherwise the algorithm is the same.

### Step 5. Killing the badness of $D_{z,2}$ .

If there are any bigons between beta and gamma curves adjacent to  $D_{z,2}$  as in Figure 13 or Figure 10 (b), also shown in Figures 19 (a) resp. (c), we do a “handleslide” (more precisely, a

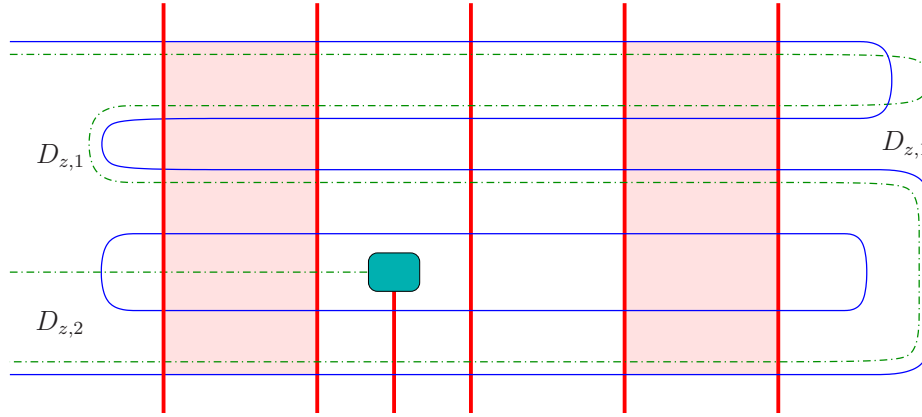


FIGURE 18. **Killing badness of  $D'$ :  $D_s$  type region - after.** Conventions and shaded regions are the same as in Figure 17. This figure is obtained from Figure 17 via a double finger move.

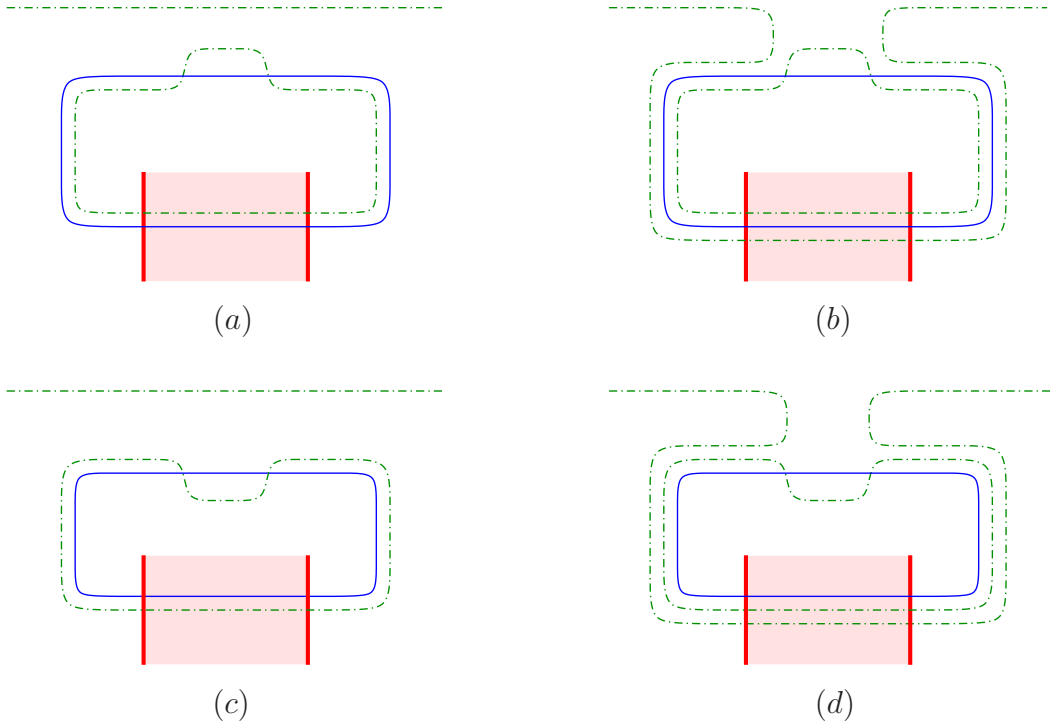


FIGURE 19. **Killing badness of  $D_{z,2}$ : special handleslides.** There might be more alpha arcs in the shaded regions.

handleslide followed by an isotopy) of  $\gamma_{g+1}$  over each  $\gamma_i$  ( $i \leq g$ ) involved as indicated in Figures 19 (b) resp. (d).

The intersection of  $\gamma_{g+1}$  and  $\alpha_{g+1}$  has the pattern as Figure 20 (a) or (b). In case (a), we do nothing. In case (b), we do the finger move as in Figure 20 (c).

Now among the possibly bad regions generated from  $D_{z,2}$ , we have a unique one whose boundary has an intersection of a beta curve with a gamma curve, namely the one near  $\beta_{g+1}$  as in Figure 21 (a). (See also Figures 14 and 18.)

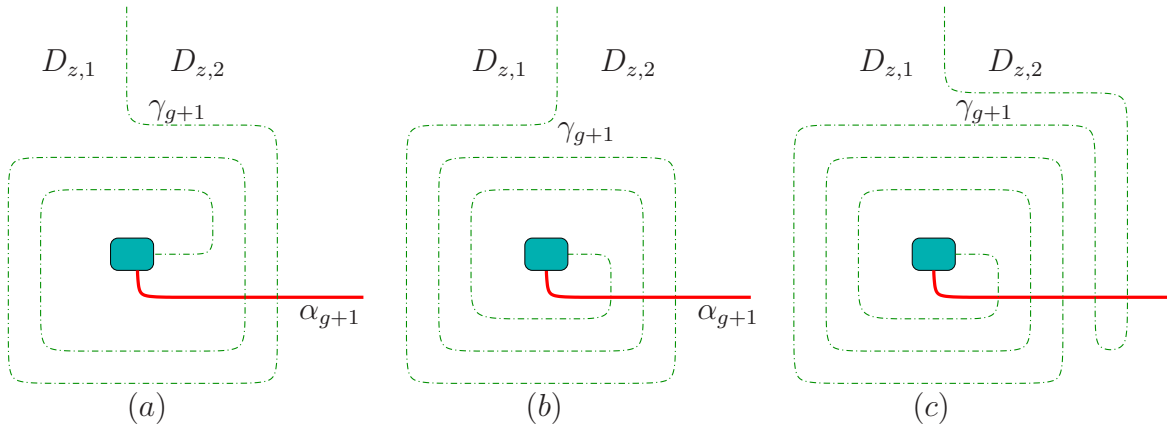


FIGURE 20. **Killing badness of  $D_{z,2}$ : two patterns.** The curve  $\gamma_{g+1}$  can rotate around the shaded oval either as in (a) or as in (b). If (b) occurs, we replace it with (c).

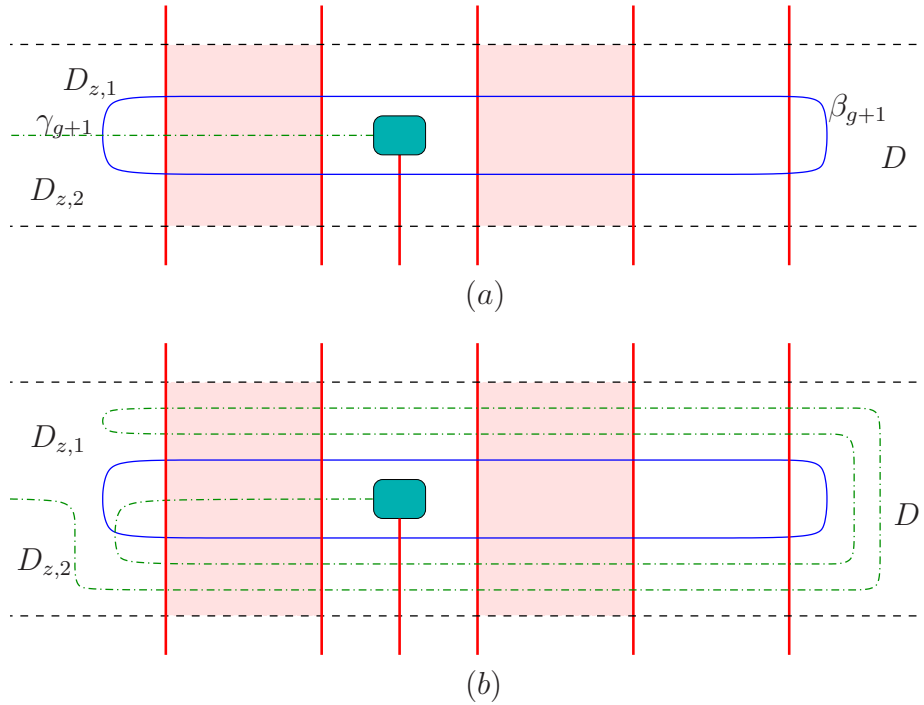


FIGURE 21. **Killing badness of  $D_{z,2}$ : special beta-gamma crossing.** The shaded area may contain several parallel alpha arcs. The dashed arcs can be beta arcs or gamma arcs depending on different cases. The region  $D$  is either a bigon or the preferred region  $D_{z,1}$ . We isotope (a) into (b) in order to remove the beta-gamma intersection point on the boundary of  $D_{z,2}$ .

We then do a finger move as in Figure 21 (b). Note that this finger move will not create any badness other than that of  $D_{z,1}$ .

After these special handleslides and finger moves, the region  $D_{z,2}$  is divided into several possibly bad regions  $R_1, \dots, R_m$ . These bad regions are all adjacent to  $D_{z,1}$  via arcs on  $\gamma_{g+1}$  and,

furthermore, there are no intersection points of beta and gamma curves on their boundaries. We seek to kill the badness of  $R_1, \dots, R_m$  using the algorithm in [9]. The algorithm there consisted of inductively decreasing a complexity function defined using the unpunctured bad regions. In our situation, we apply a simple modification of the algorithm to the Heegaard diagram made of the alpha and the gamma curves; the modification consists of the fact that we do not deal with the bad region(s)  $D_*$  (or  $D_{*,1}$  and  $D_{*,2}$ ), but rather only seek to eliminate the badness of  $R_1, \dots, R_m$ ; thus, in the complexity function we do not include terms that involve the badness and distance of  $D_*$  (or  $D_{*,1}$  and  $D_{*,2}$ ).

Since all the  $R_i$ 's are adjacent to the preferred (punctured) region  $D_{z,1}$  via arcs on  $\gamma_{g+1}$ , the algorithm in [9] prescribes doing finger moves of  $\gamma_{g+1}$  through alpha curves, and (possibly) handleslides of  $\gamma_{g+1}$  over other gamma curves. We do all these moves in such a way as not to tamper with the arrangements of twin beta-gamma curves, i.e. as not to introduce any new intersection points between  $\gamma_{g+1}$  and  $\beta_i$ , for any  $i \leq g$ . (In other words, we can think of fattening  $\gamma_1, \dots, \gamma_g$  before applying the algorithm, so that they include their respective twin beta curves.) In particular, regions of type  $D_s$  are treated as bigons.

The fact that the algorithm in [9] can be applied in this fashion is based on the following two observations:

- Our fingers or handleslides will not pass through the regions adjacent to  $\beta_{g+1}$ , except possibly  $D_{z,1}$  itself. (This is one benefit of the modification performed in Figure 21.)
- We will not reach any squares between  $\beta_i$  and  $\gamma_i$ , nor the “narrow” squares created in Figure 19.

In the end, all the badness of  $R_1, \dots, R_m$  is killed. We arrive at a Heegaard diagram which might still have some bad regions coming from regions of type  $D_s$ , as in Figure 22 (a). We kill these bad regions using the finger moves indicated in Figure 22 (b).

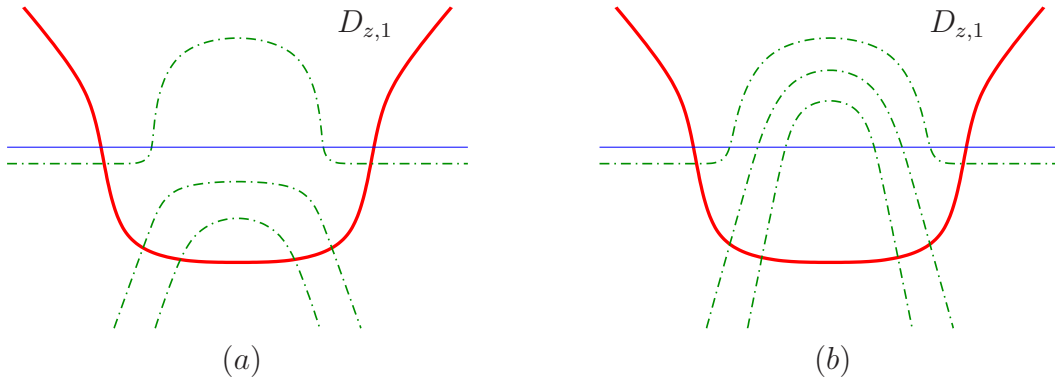


FIGURE 22. **Killing badness of special bad regions.** We isotope the gamma curves to kill the hexagon in (a).

After these moves, the only remaining bad regions are  $D_*$  (or  $D_{*,1}$  and  $D_{*,2}$ ), and the preferred bad region  $D_{z,1}$ .

### Step 6. Killing the badness of $D_*$ (or $D_{*,i}$ ).

Our remaining task is to kill the badness of  $D_*$  or  $D_{*,i}$ . Recall that depending on the pattern of the intersection of  $\alpha_{g+1}$  and  $\gamma_{g+1}$  (cf. Figure 20), there are two cases: either we have an octagon bad region  $D_*$ , or two hexagon bad regions  $D_{*,1}$  and  $D_{*,2}$ .

In the first case, one possibility is that a neighborhood of  $\alpha_{g+1} \cup \beta_{g+1} \cup \gamma_{g+1}$  looks as in Figure 23. We then do the finger moves indicated in Figure 24. It is routine to check that the new diagram is isotopic to the one in Figure 23.

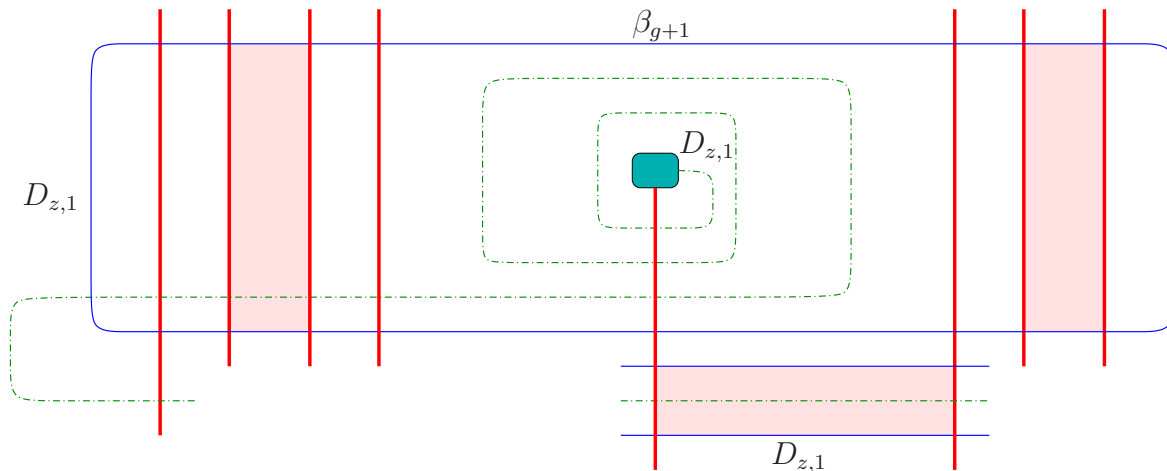


FIGURE 23. **The bad region  $D_*$ .** Conventions are as before. Lightly shaded regions mean several parallel arcs.

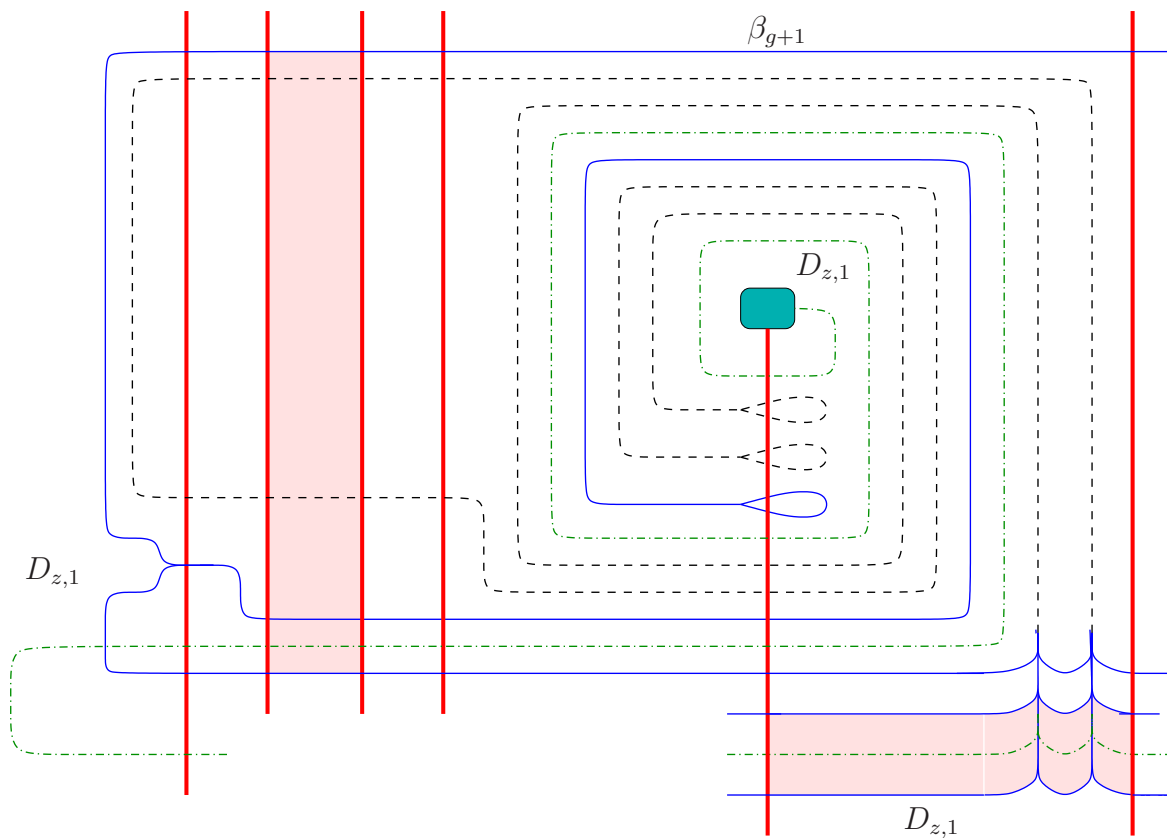


FIGURE 24. **Killing badness of  $D_*$ .** We push two multiple fingers (containing several beta and gamma curves) from the bottom right of the diagram, and a single finger from the left. We are using the train-track convention, cf. Figure 25 below.



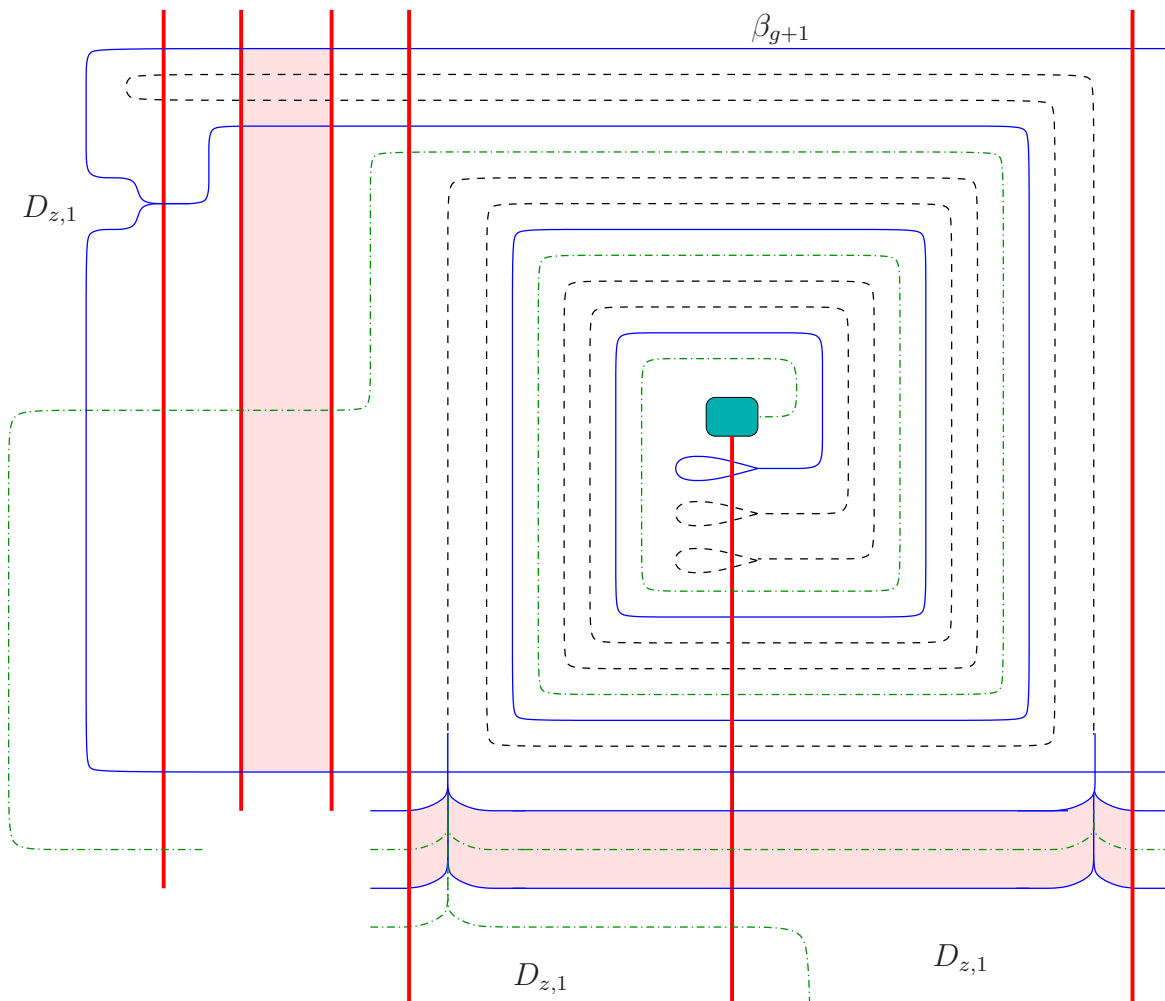


FIGURE 27. **Killing badness of  $D_{*,1}$  and  $D_{*,2}$ .** In this case, we again push two multiple fingers from the bottom, but starting from two different sides of  $\alpha_{g+1}$ . As before, we also push a finger from the left.

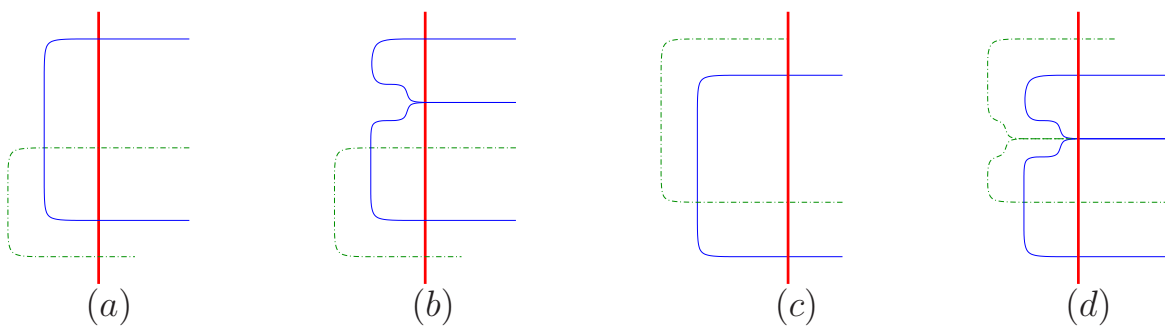


FIGURE 28. **A variation.** On the left of Figures 23 and 26, we might have the picture (c) rather than (a). We then do the finger move in (d) instead of (b). The region on the left is always  $D_{z,1}$ .

**3.3. Several two-handle additions.** We now explain how the arguments in this section can be extended to a cobordism  $W$  which consists of the addition of several two-handles. We view  $W$  as surgery along a link  $L \subset Y$  of  $l$  components.

We start with a multi-pointed Heegaard diagram  $(\Sigma, \alpha, \beta, \mathbf{z})$ , together with another set of base-points  $\mathbf{w} = \{w_1, \dots, w_l\}$  describing the pair  $L \subset Y$ , as in [3]. Each of the two sets of curves ( $\alpha$  and  $\beta$ ) has  $g + l - 1$  elements.

Applying the algorithm in [9] we can make this diagram nice, i.e. such that all regions not containing one of the  $z$ 's are either bigons or rectangles. For  $i = 1, \dots, l$ , we denote by  $D_{z_i}$  the region containing  $z_i$ .

As in Step 1 of Section 3.2, we inductively remove intersection points between the various components of the projection of  $L$  to  $\Sigma$ . This projection consists of arcs  $c_i$  and  $c'_i$  with endpoints at  $z_i$  and  $w_i$  ( $i = 1, \dots, l$ ), such that each  $c_i$  is disjoint from the beta curves, and each  $c'_i$  is disjoint from the alpha curves. Instead of Figure 8 we have the situation in Figure 29. Again, we stabilize and perform an isotopy to obtain a good diagram with one fewer intersection point, as in Figure 9. Iterating this process (on all link components), we can assume that the projection of  $L$  is embedded in the Heegaard surface.

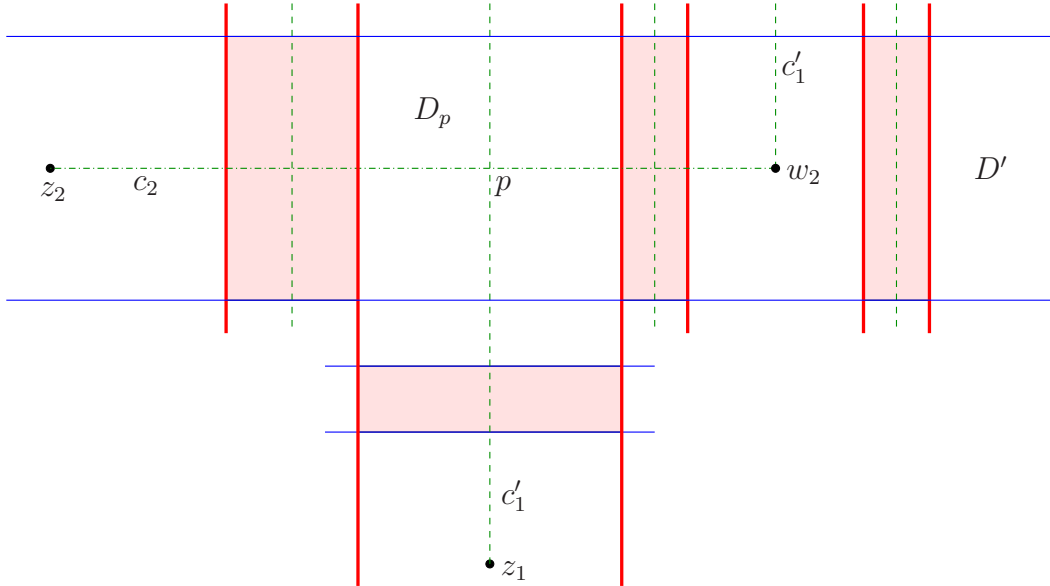


FIGURE 29. **Projection of the link to the Heegaard surface.** The point  $p$  is the point on the dashed  $c'_1$  curve closest to  $z_1$  where an intersection with any of the  $c_i$  curves (in our case  $c_2$ ) takes place.

We then add twin gamma curves as in Step 2 of Section 3.2. For this we need to do several isotopies of the beta curves as in Figure 12. In that figure, if the region on the top left is  $D_{z_i}$ , the one on the right might be  $D_{z_j}$  for  $j \neq i$ ; however, the isotopy can be done as before.

Next, we stabilize the Heegaard diagram  $l$  times (once for each link component) to obtain a triple diagram for the cobordism, as in Step 3 of Section 3.2. We then do the analogue of Step 4 by pushing  $l$  fingers to kill the badness of the regions of type  $D'$ . Since the fingers only pass through rectangles, they do not intersect each other. The only change is that in Figures 17 and 18, the region on the very right may contain a different puncture  $z_i$  than the one on the left.

At the end of Step 4, the beta curves split the Heegaard surface into  $l$  connected components  $C_1, \dots, C_l$ . We then do the analogue of Step 5 in Section 3.2. Note that this step (except for the very last bit, Figure 22) only involves moving gamma curves through alpha curves. (Here,

we think of the move in Figure 19 as a single step, rather than as a handleslide followed by an isotopy.) Therefore, we can perform the moves in this step once for each connected component of  $L$ , independently of each other, because the moves take place in the corresponding component  $C_i$ . In the situation considered in Figure 22, the gamma curves cross a beta curve; however, the special region  $D_s$  is part of a unique  $C_i$ , so we can perform the isotopy of the gamma curves as before, without interference from another  $C_j$ .

Finally, for Step 6, note that in all the previous steps we have not destroyed the property that the projection of  $L$  to the Heegaard surface is embedded. More precisely, in the part of the stabilized Heegaard diagram shown in Figure 14, we take a component of the link projection to be a loop starting in  $D_*$ , near the upper foot of the handle, going down along  $\alpha_{g+1}$  until it reaches  $D_{z,1}$ , then going inside  $D_{z,1}$  until it reaches the intersection of  $\gamma_{g+1}$  and  $\beta_{g+1}$ , and then going along a sub-arc of  $\gamma_{g+1}$  to its original departure. These paths remain embedded, and disjoint from each other, throughout Steps 4 and 5. (Indeed, neither  $\beta_{g+1}$  nor this sub-arc of  $\gamma_{g+1}$  is moved during these steps.) It then suffices to note the finger moves in Step 6 take place in a neighborhood of the projection of the corresponding link component (the path considered above). Therefore, these finger moves can be done without interfering with each other. The result is a nice multi-pointed triple Heegaard diagram for  $W$ .

## 4. ONE- AND THREE-HANDLE ADDITIONS

4.1.  $H_1(Y)/tors$ -action in nice diagrams. Let  $\mathfrak{s}_0$  denote the torsion  $\text{Spin}^c$ -structure on  $\#^n S^1 \times S^2$ . Recall that for any  $\text{Spin}^c$ -structure  $\mathfrak{s}$  on a 3-manifold  $Y$  there is an isomorphism

$$(5) \quad \widehat{HF}(Y, \mathfrak{s}) \otimes H_*(T^n) \xrightarrow{\cong} \widehat{HF}(Y \# (\#^n S^1 \times S^2), \mathfrak{s} \# \mathfrak{s}_0).$$

Let  $\theta$  be a generator of the top-graded part of  $H_*(T^n)$ , and  $\eta$  a generator of the bottom-graded part. In this section we prove that given a nice Heegaard diagram for  $Y \# (\#^n S^1 \times S^2)$  and a splitting  $H^1(Y \# (\#^n S^1 \times S^2)) \cong H^1(Y) \oplus H^1(\#^n S^1 \times S^2)$  one can identify combinatorially the images of  $\widehat{HF}(Y, \mathfrak{s}) \otimes \theta$  and of  $\widehat{HF}(Y, \mathfrak{s}) \otimes \eta$  under the isomorphism (5). To do so, we will use the  $H_1(Y)/tors$ -action on  $\widehat{HF}$ .

We start by reviewing the definition of the  $H_1(Y)/tors$ -action. We will use the construction from [1, Section 8.1] rather than the original construction in [5, Section 4.2.5] because it is more transparently combinatorial.

Suppose that  $x$  and  $y$  are generators of  $\widehat{CF}(\Sigma, \alpha, \beta, \mathbf{z})$ , i.e., intersection points between  $\mathbb{T}_\alpha$  and  $\mathbb{T}_\beta$  in  $\text{Sym}^{g+k}(\Sigma)$ . Let  $\hat{\pi}_2(x, y)$  denote the homotopy classes of Whitney disks connecting  $x$  to  $y$  in  $\text{Sym}^{g+k}(\Sigma \setminus \mathbf{z})$ . If  $x$  and  $y$  represent the same  $\text{Spin}^c$ -structure then  $\hat{\pi}_2(x, y)$  is an affine copy of  $H_2(Y) \oplus \mathbb{Z}^k$ . (Here, as always, the cardinality of  $\mathbf{z}$  is  $k + 1$ .) Further, for any  $x \in \mathbb{T}_\alpha \cap \mathbb{T}_\beta$ ,  $H_2(Y)$  is canonically identified with a subgroup of  $\hat{\pi}_2(x, x)$ .

Given generators  $x$  and  $y$  of  $\widehat{CF}(\Sigma, \alpha, \beta, \mathbf{z})$  and  $\phi \in \hat{\pi}_2(x, y)$  let  $\mathcal{M}(\phi)$  denote the moduli space of holomorphic disks in the homotopy class  $\phi$ , with respect to some generic almost complex structure  $J$ . Recall that the differential of  $x$  is given by

$$\partial x = \sum_{y \in \mathbb{T}_\alpha \cap \mathbb{T}_\beta} \sum_{\substack{\phi \in \hat{\pi}_2(x, y) \\ \mu(\phi)=1}} \#(\mathcal{M}(\phi)/\mathbb{R}) y.$$

It was proved in [9] that in a nice Heegaard diagram, if  $\mu(\phi) = 1$  then the number of elements of  $\mathcal{M}(\phi)/\mathbb{R}$  can be determined combinatorially. Specifically, for a nice Heegaard diagram, elements of  $\mathcal{M}(\phi)/\mathbb{R}$  are just embedded squares or bigons in  $(\Sigma, \alpha \cup \beta)$ .

The  $H_1(Y)/tors$ -action is defined similarly to the differential. Fix  $x_0 \in \mathbb{T}_\alpha \cap \mathbb{T}_\beta$  representing the  $\text{Spin}^c$ -structure  $\mathfrak{s}$ . For every other  $x$  representing  $\mathfrak{s}$  choose an element  $\phi_x \in \hat{\pi}_2(x, x_0)$ . With these choices, the map  $\hat{\pi}_2(x_0, x_0) \rightarrow \hat{\pi}_2(x, y)$  given by  $\phi \mapsto \phi_y * \phi * \overline{\phi_x}$  identifies  $H_2(Y)$  as a subgroup of  $\hat{\pi}_2(x, y)$  for any  $x, y$  in the  $\text{Spin}^c$ -structure  $\mathfrak{s}$ . (The operator  $*$  denotes concatenation of disks, and  $\bar{\phantom{x}}$  the map which takes a disk to its inverse.)

Now, fix an element  $\zeta \in H_1(Y)/tors \cong \text{Hom}(H_2(Y), \mathbb{Z})$ . With the identifications of the previous paragraph,  $\zeta$  gives a map  $\hat{\pi}_2(x, y) \rightarrow \mathbb{Z}$  for any generators  $x$  and  $y$  representing the  $\text{Spin}^c$ -structure  $\mathfrak{s}$ . Now, define

$$A_\zeta(x) = \sum_{y \in \mathbb{T}_\alpha \cap \mathbb{T}_\beta} \sum_{\substack{\phi \in \hat{\pi}_2(x, y) \\ \mu(\phi)=1}} \#(\mathcal{M}(\phi)/\mathbb{R}) \zeta(\phi) y.$$

It is not hard to check that  $A_\zeta$  is a chain map, and is independent of the choices made; see [1, Section 8.1]. Further, since for a nice Heegaard diagram the counts of index 1 holomorphic disks are combinatorial, it is clear that  $A_\zeta$  can be computed combinatorially in a nice Heegaard diagram.

Returning to the situation of this paper, suppose we have a 3-manifold of the form  $Y \# (\#^n S^1 \times S^2)$ . Then

$$\widehat{HF}(Y \# (\#^n S^1 \times S^2), \mathfrak{s} \# \mathfrak{s}_0) \cong \widehat{HF}(Y, \mathfrak{s}) \otimes \widehat{HF}(\#^n S^1 \times S^2, \mathfrak{s}_0),$$

as  $\mathbb{F}[(H_1(Y)/tors) \oplus H_1(\#^n S^1 \times S^2)]$ -modules. Here, the action of  $H_1(\#^n S^1 \times S^2)$  on  $\widehat{HF}(Y, \mathfrak{s})$  is trivial, as is the action of  $H_1(Y)/tors$  on  $\widehat{HF}(\#^n S^1 \times S^2, \mathfrak{s}_0)$ . Further, it is easy to check that

the action of  $H_1(\#^n S^1 \times S^2)/tors \cong H^1(T^n)$  on  $\widehat{HF}(\#^n S^1 \times S^2, \mathfrak{s}_0) \cong H_*(T^n)$  is exactly the given by cap product  $\cap : H^1(T^n) \otimes H_*(T^n) \rightarrow H_{*-1}(T^n)$ .

We have, therefore, proved the following proposition.

**Proposition 4.1.** *Suppose  $(\Sigma, \alpha, \beta, \mathbf{z})$  is a multi-pointed Heegaard diagram for  $Y\#(\#^n S^1 \times S^2)$ . Let  $\theta \in \widehat{HF}(\#^n S^1 \times S^2, \mathfrak{s}_0)$  be a generator of the highest-graded nonzero group. Then the subgroup  $\widehat{HF}(Y, \mathfrak{s}) \otimes \theta$  of  $\widehat{HF}(Y\#(\#^n S^1 \times S^2), \mathfrak{s}\#\mathfrak{s}_0)$  consists of those elements  $x$  such that  $A_\zeta(x) \neq 0$  for any  $\zeta \neq 0 \in H_1(\#^n S^1 \times S^2)$ . If  $(\Sigma, \alpha, \beta, \mathbf{z})$  is nice then this is a combinatorial condition.*

*Dually, suppose  $(\Sigma, \alpha, \gamma, \mathbf{z})$  is a multi-pointed Heegaard diagram for  $Y\#(\#^n S^1 \times S^2)$ . Let  $\eta \in \widehat{HF}(\#^n S^1 \times S^2, \mathfrak{s}_0)$  be a generator of the lowest-graded nonzero group. Then the subgroup  $\widehat{HF}(Y, \mathfrak{s}) \otimes \eta$  of  $\widehat{HF}(Y\#(\#^n S^1 \times S^2), \mathfrak{s}\#\mathfrak{s}_0)$  consists of those elements  $x$  such that  $A_\zeta(x) = 0$  for all  $\zeta \in H_1(\#^n S^1 \times S^2)$ . If  $(\Sigma, \alpha, \gamma, \mathbf{z})$  is nice then this is a combinatorial condition.*

**4.2. One- and three-handle additions.** Suppose that  $W_1$  is a cobordism from  $Y_0$  to  $Y_1$  built entirely from 1-handles. Let  $\mathfrak{t}$  be a  $\text{Spin}^c$ -structure on  $W_1$ . In [7, Section 4.3], the map  $\hat{F}_{W_1, \mathfrak{t}} : \widehat{HF}(Y_0, \mathfrak{t}|_{Y_0}) \rightarrow \widehat{HF}(Y_1, \mathfrak{t}|_{Y_1})$  is constructed as follows. Since  $W_1$  consists entirely of 1-handles,  $Y_1 \cong Y_0\#(\#^n S^1 \times S^2)$  (where  $n$  is the number of 1-handles of  $W_1$ ). Further, the restriction of  $\mathfrak{t}$  to the  $(S^1 \times S^2)$ -summands in  $Y_1$  is torsion. It follows that  $\widehat{HF}(Y_1, \mathfrak{t}|_{Y_1}) \cong \widehat{HF}(Y_0, \mathfrak{t}|_{Y_0}) \otimes H_*(T^n)$ . Let  $\theta$  be a generator of the top-graded part of  $H_*(T^n)$ . Then define  $\hat{F}_{W_1, \mathfrak{t}}(x) = x \otimes \theta$ . We extend this definition to the multi-pointed case as follows. Suppose that  $(\Sigma, \alpha, \beta, \mathbf{z})$  is a multi-pointed Heegaard diagram for  $Y_1$ . Then for any  $\text{Spin}^c$ -structure  $\mathfrak{s}$  on  $Y_1$ ,

$$(6) \quad \widehat{HF}(\Sigma, \alpha, \beta, \mathbf{z}, \mathfrak{s}) \cong \widehat{HF}(Y_1, \mathfrak{s}) \otimes H_*(T^k).$$

Define a map  $\hat{F}_{W_1, \mathfrak{t}} : \widehat{HF}(Y_0, \mathfrak{t}|_{Y_0}) \otimes H_*(T^k) \rightarrow \widehat{HF}(\Sigma, \alpha, \beta, \mathbf{z}, \mathfrak{t}|_{Y_1})$  by tensoring  $\hat{F}_{W_1, \mathfrak{t}} : \widehat{HF}(Y_0, \mathfrak{t}|_{Y_0}) \rightarrow \widehat{HF}(Y_1, \mathfrak{t}|_{Y_1})$  with  $Id : H_*(T^k) \rightarrow H_*(T^k)$ . Note that while the extension itself depends on a choice of decomposition (6), the image does not.

Dually, suppose that  $W_3$  is a cobordism from  $Y_2$  to  $Y_3$  built entirely from 3-handles. Let  $\mathfrak{t}$  be a  $\text{Spin}^c$ -structure on  $W_2$ . In [7, Section 4.3], a map  $\hat{F}_{W_3, \mathfrak{t}} : \widehat{HF}(Y_2, \mathfrak{t}|_{Y_2}) \rightarrow \widehat{HF}(Y_3, \mathfrak{t}|_{Y_3})$  is constructed as follows. Since  $W_3$  consists entirely of 3-handles,  $Y_2 \cong Y_3\#(\#^m S^1 \times S^2)$  (where  $m$  is the number of 3-handles of  $W_3$ ). Further, the restriction of  $\mathfrak{t}$  to the  $(S^1 \times S^2)$ -summands in  $Y_2$  is torsion. It follows that  $\widehat{HF}(Y_2, \mathfrak{t}|_{Y_2}) \cong \widehat{HF}(Y_3, \mathfrak{t}|_{Y_3}) \otimes H_*(T^m)$ . Let  $\eta$  be a generator of the top-graded part of  $H_*(T^m)$ . Then define  $\hat{F}_{W_3, \mathfrak{t}}(x \otimes \eta) = x$  while  $\hat{F}_{W_3, \mathfrak{t}}(x \otimes \omega) = 0$  for any other generator  $\omega$  of  $H_*(T^m)$ . Again, we extend this definition to the multi-pointed case by tensoring with the identity map  $Id : H_*(T^k) \rightarrow H_*(T^k)$ . While the extension itself depends on a choice of decomposition (6), the kernel does not.

The following proposition is immediate from Proposition 4.1

**Proposition 4.2.** *Suppose that  $W_1$  is a cobordism from  $Y_0$  to  $Y_1$  built entirely from 1-handles. Suppose  $(\Sigma, \alpha, \beta, \mathbf{z})$  is a nice  $k$ -pointed Heegaard diagram for  $Y_1$ ,  $\mathfrak{t}$  is a  $\text{Spin}^c$ -structure on  $W_1$ , and  $\hat{F}_{W_1, \mathfrak{t}} : \widehat{HF}(Y_0, \mathfrak{t}|_{Y_0}) \otimes H_*(T^k) \rightarrow \widehat{HF}(\Sigma, \alpha, \beta, \mathbf{z}, \mathfrak{t}|_{Y_1})$  is the map induced by  $(W_1, \mathfrak{t})$ . Then the image of  $\hat{F}_{W_1, \mathfrak{t}}$  is exactly the subgroup of  $\widehat{HF}(\Sigma, \alpha, \beta, \mathbf{z}, \mathfrak{t}|_{Y_0})$  consisting of those elements  $x$  such that  $A_\zeta(x) \neq 0$  for any  $\zeta \neq 0 \in H_1(\#^n S^1 \times S^2)$ . This is a combinatorial condition which can be checked in  $(\Sigma, \alpha, \beta, \mathbf{z})$ .*

*Dually, suppose that  $W_3$  is a cobordism from  $Y_2$  to  $Y_3$  built entirely from 1-handles. Suppose that  $(\Sigma, \alpha, \gamma, \mathbf{z})$  is a nice  $k$ -pointed Heegaard diagram for  $Y_2$ ,  $\mathfrak{t}$  is a  $\text{Spin}^c$ -structure on  $W_2$ , and  $\hat{F}_{W_3, \mathfrak{t}} : \widehat{HF}(\Sigma, \alpha, \gamma, \mathbf{z}, \mathfrak{t}|_{Y_2}) \rightarrow \widehat{HF}(Y_3, \mathfrak{t}|_{Y_3}) \otimes H_*(T^k)$  is the map induced by  $(W_3, \mathfrak{t})$ . Then the kernel of  $\hat{F}_{W_3, \mathfrak{t}}$  consists of those elements  $x$  such that  $A_\zeta(x) \neq 0$  for some  $\zeta \in H_1(\#^n S^1 \times S^2)$ . This is a combinatorial condition which can be checked in  $(\Sigma, \alpha, \gamma, \mathbf{z})$ .*

### 4.3. Putting it all together.

**Theorem 4.3.** *Let  $W$  be a cobordism from  $Y_0$  to  $Y_3$ , and  $\mathfrak{t}$  a  $\text{Spin}^c$ -structure on  $W$ . Then in each grading  $i$  the rank of  $\widehat{F}_{W,s} : \widehat{HF}_i(Y_0, \mathfrak{t}|_{Y_0}) \rightarrow \widehat{HF}_*(Y_3, \mathfrak{t}|_{Y_3})$  can be computed combinatorially.*

*Proof.* Choose a self-indexing Morse function on  $W$ . This decomposes  $W$  as a collection of one-handle additions which together form a cobordism  $W_1$ , followed by some two-handle additions forming a cobordism  $W_2$ , and three-handle additions forming a cobordism  $W_3$ , in this order. Let  $Y_1$  and  $Y_2$  be the intermediate three-manifolds, so that

$$W = W_1 \cup_{Y_1} W_2 \cup_{Y_2} W_3.$$

The map  $\widehat{F}_{W,\mathfrak{t}}$  is, by definition, the composition  $\widehat{F}_{W_3,\mathfrak{t}|_{W_3}} \circ \widehat{F}_{W_2,\mathfrak{t}|_{W_2}} \circ \widehat{F}_{W_1,\mathfrak{t}|_{W_1}}$ . Here,  $\widehat{F}_{W_2,\mathfrak{t}|_{W_2}}$  counts holomorphic triangles; as discussed in Section 4.2, the maps  $\widehat{F}_{W_1,\mathfrak{t}|_{W_1}}$  and  $\widehat{F}_{W_3,\mathfrak{t}|_{W_3}}$  are more simple minded.

Using the algorithm from Section 3.3 we obtain a nice triple Heegaard diagram  $(\Sigma, \boldsymbol{\alpha}, \boldsymbol{\beta}, \boldsymbol{\gamma}, \mathbf{z})$  for  $W_1$ . Note that by Lemma 2.2,  $(\Sigma, \boldsymbol{\alpha}, \boldsymbol{\beta}, \mathbf{z})$  and  $(\Sigma, \boldsymbol{\alpha}, \boldsymbol{\gamma}, \mathbf{z})$  are also nice. In light of Corollary 3.2, by Proposition 2.3 the map

$$\widehat{F}_{W_2,\mathfrak{t}|_{W_2}} : \widehat{HF}(\Sigma, \boldsymbol{\alpha}, \boldsymbol{\beta}, \mathbf{z}, \mathfrak{t}|_{Y_1}) \rightarrow \widehat{HF}(\Sigma, \boldsymbol{\alpha}, \boldsymbol{\gamma}, \mathbf{z}, \mathfrak{t}|_{Y_2})$$

can be computed combinatorially.

Suppose that  $\mathbf{z}$  consists of  $k$  points. By Proposition 4.2, one can determine combinatorially the image of  $\widehat{F}_{W_1,\mathfrak{t}|_{W_1}} : \widehat{HF}(Y_1) \otimes H_*(T^k) \rightarrow \widehat{HF}(\Sigma, \boldsymbol{\alpha}, \boldsymbol{\beta}, \mathbf{z}, \mathfrak{t}|_{Y_2})$ . Therefore, one can compute combinatorially the image  $I$  of  $\widehat{F}_{W_2,\mathfrak{t}|_{W_2}} \circ \widehat{F}_{W_1,\mathfrak{t}|_{W_1}}$  inside  $\widehat{HF}(\Sigma, \boldsymbol{\alpha}, \boldsymbol{\gamma}, \mathbf{z}, \mathfrak{t}|_{Y_2})$ . By the second half of Proposition 4.2, one can also compute the kernel  $K$  of  $\widehat{F}_{W_3,\mathfrak{t}|_{W_3}} : \widehat{HF}(Y_2) \rightarrow \widehat{HF}(Y_3)$ . Now, the rank of  $\widehat{F}_{W,\mathfrak{t}}$  is

$$\frac{1}{2^k} (\dim(I) - \dim(I \cap K)).$$

This proves the result. □

## REFERENCES

- [1] R. Lipshitz. A cylindrical reformulation of Heegaard Floer homology. *Geom. Topol.*, 10:955–1097, 2006.
- [2] C. Manolescu, P. S. Ozsváth, and S. Sarkar. A combinatorial description of knot Floer homology. Preprint, math.GT/0607691.
- [3] P. S. Ozsváth and Z. Szabó. Holomorphic disks and link invariants. Preprint, math.GT/0512286.
- [4] P. S. Ozsváth and Z. Szabó. Holomorphic disks and knot invariants. *Adv. Math.*, 186(1):58–116, 2004.
- [5] P. S. Ozsváth and Z. Szabó. Holomorphic disks and topological invariants for closed three-manifolds. *Ann. of Math. (2)*, 159(3):1027–1158, 2004.
- [6] P. S. Ozsváth and Z. Szabó. Holomorphic disks and three-manifold invariants: properties and applications. *Ann. of Math. (2)*, 159(3):1159–1245, 2004.
- [7] P. S. Ozsváth and Z. Szabó. Holomorphic triangles and invariants for smooth four-manifolds. *Adv. Math.*, 202(2):326–400, 2006.
- [8] S. Sarkar. Maslov index of holomorphic triangles. Preprint, math.GT/0609673.
- [9] S. Sarkar and J. Wang. A combinatorial description of some Heegaard Floer homologies. Preprint, math.GT/0607777.

DEPARTMENT OF MATHEMATICS, COLUMBIA UNIVERSITY, NEW YORK, NY 10027  
*E-mail address:* lipshitz@math.columbia.edu

DEPARTMENT OF MATHEMATICS, COLUMBIA UNIVERSITY, NEW YORK, NY 10027  
*E-mail address:* cm@math.columbia.edu

DEPARTMENT OF MATHEMATICS, UNIVERSITY OF CALIFORNIA AT BERKELEY, BERKELEY, CA 94720  
*E-mail address:* wang@math.berkeley.edu